AD-A038 630 OHIO STATE UNIV COLUMBUS DEPT OF GEODETIC SCIENCE F/G 8/5
RECOVERY OF MEAN GRAVITY ANOMALIES FROM SATELLITE-SATELLITE RAN--ETC(U)
SEP 76 R RUMMEL, D P HAJELA, R H RAPP F19628-76-C-0010
UNCLASSIFIED DGS-248 AFGL-TR-76-0291 NL

| OF |
AD
A038630

END

DATE
FILMED
5-77

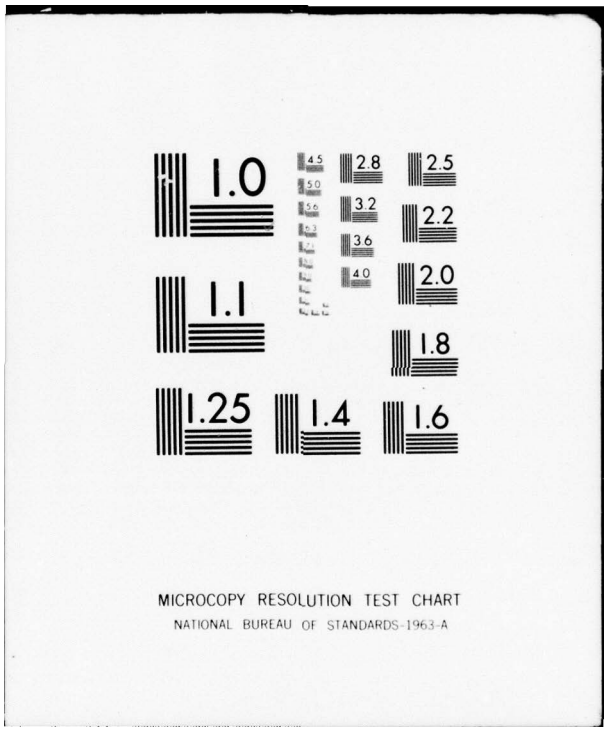
1.0
1.1
1.25
1.4
1.6
1.8
2.0
2.2
2.5
2.8
3.2
3.6
4.0
4.5
5.0
5.6
MICROCOPY RESOLUTION TEST CHART
NATIONAL BUREAU OF STANDARDS-1963-A

AFGL-TR-76-0291

RECOVERY OF MEAN GRAVITY ANOMALIES FROM SATELLITE - SATELLITE RANGE RATE DATA USING LEAST SQUARES COLLOCATION

Reiner Rummel
D. P. Hajela
Richard H. Rapp

The Ohio State University
Research Foundation
Columbus, Ohio 43212

September 1976

Scientific Report No. 7

AIR FORCE GEOPHYSICS LABORATORY
AIR FORCE SYSTEMS COMMAND
UNITED STATES AIR FORCE
HANSCOM AFB, MASSACHUSETTS 01731

Qualified requestors may obtain additional copies from the Defense Documentation Center. All others should apply to the National Technical Information Service.

Unclassified

SECURITY CLASSIFICATION OF THIS PAGE (When Data Entered)

REPORT DOCUMENTATION PAGE	READ INSTRUCTIONS BEFORE COMPLETING FORM
1. REPORT NUMBER: AFGL-TR-76-0291	2. GOVT ACCESSION NO.
3. RECIPIENT'S CATALOG NUMBER	
4. TITLE (and Subtitle): RECOVERY OF MEAN GRAVITY ANOMALIES FROM SATELLITE - SATELLITE RANGE RATE DATA USING LEAST SQUARES COLLOCATION.	5. TYPE OF REPORT & PERIOD COVERED: Scientific. Interim rept. Scientific Report No. 7
	6. PERFORMING ORG. REPORT NUMBER: Geodetic Science 248
7. AUTHOR(s): Reiner Rummel, D. P. Hajela, Richard H. Rapp	8. CONTRACT OR GRANT NUMBER(s): F19628-76-C-0010
9. PERFORMING ORGANIZATION NAME AND ADDRESS: Department of Geodetic Science, The Ohio State University - 1958 Neil Avenue, Columbus, Ohio 43210	10. PROGRAM ELEMENT, PROJECT, TASK AREA & WORK UNIT NUMBERS: 62101F, 7600-0302, 03
11. CONTROLLING OFFICE NAME AND ADDRESS: Air Force Geophysics Laboratory, Hanscom AFB, Massachusetts 01731, Contract Monitor: Bela Szabo/LW	12. REPORT DATE: September 1976
	13. NUMBER OF PAGES: 67
14. MONITORING AGENCY NAME & ADDRESS (if different from Controlling Office): DGS-248, Scientific-7	15. SECURITY CLASS. (of this report): Unclassified
67 p.	15a. DECLASSIFICATION/DOWNGRADING SCHEDULE

16. DISTRIBUTION STATEMENT (of this Report)

A-Approved for public release; distribution unlimited

17. DISTRIBUTION STATEMENT (of the abstract entered in Block 20, if different from Report)

DDC REPRODUCED APR 25 1977 USGS

18. SUPPLEMENTARY NOTES

TECH, OTHER

19. KEY WORDS (Continue on reverse side if necessary and identify by block number)

Gravity anomalies, geodesy, satellite to satellite data, collocation

20. ABSTRACT (Continue on reverse side if necessary and identify by block number)

Range rate data between two satellites can be used to determine acceleration along the connecting line between two satellites by numerically differentiating an analytic representation of this data. Using a reference potential field this acceleration can be interpreted to be a derivative of the disturbing potential along the line of the satellites. Using geometric techniques, the radial component of the disturbing potential can be estimated. This component can then be incorporated in the deter-

cover

DD FORM 1 JAN 73 1473 EDITION OF 1 NOV 65 IS OBSOLETE

Unclassified 400 254

SECURITY CLASSIFICATION OF THIS PAGE (When Data Entered)

mination of mean gravity anomalies at the surface of the earth using least squares collocation and theoretical covariance functions. This paper discusses the theoretical basis of the above procedures and describes two simulation studies performed.

In the first, postulated data surrounding a 5° equal area block and a 2° x 2° block was used to estimate the accuracy in which the anomaly could be recovered. For example, with acceleration data having an accuracy of ±1 mgal, a 5° anomaly could be determined with an accuracy of ±4 mgals with the low satellite at 250 km, and ±8 mgals with the low satellite at 850 km. A comprehensive simulation experiment was then performed to check the actual recovery of postulated anomalies determined from defined sets of potential coefficients. Assuming known orbits the recovery of the unknown anomalies was accomplished to about ±2 mgals. When orbits errors were introduced the errors increased but could properly be controlled through assignment of data accuracies.

The promising results of this study indicate that least squares collocation techniques can be advantageously applied to this type of anomaly recovery avoiding the instability of the downward continuation problem that exists in other methods of anomaly recovery from this data type.

Foreword

This report was prepared by Dr. Reiner Rummel and Dr. D. P. Hajela, Research Associates, and Dr. Richard H. Rapp, Professor, of the Department of Geodetic Science, The Ohio State University, under Air Force Contract No. F19628-76-C-0010, The Ohio State University Research Foundation Project No. 4214B1. The contract covering this research is administered by the Air Force Geophysics Laboratory, L. G. Hanscom Air Force Base, Massachusetts, with Mr. Bela Szabo, Contract Monitor.

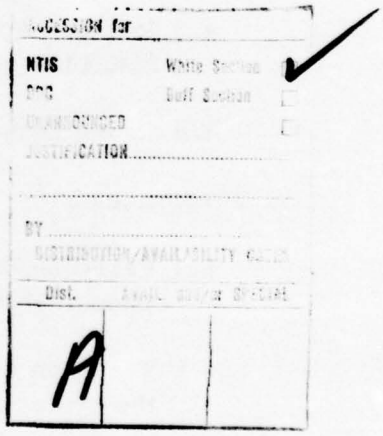

TABLE OF CONTENTS

Foreword iii

0. Introduction 1

1. Theoretical Discussion 1

2. The Covariance Functions 12

3. Preliminary Simulation Studies 15

4. Simulation of Data 18

4.1 Residual 10° and 5° Equal Area Mean Anomalies 20

4.2 Residual Range Rate Between Relay and Close Satellites 24

4.3 Residual Acceleration Between Relay and Close Satellites 26

4.4 Radial Derivative of the Disturbing Potential 29

5. Prediction of 10° Equal Area Residual Anomalies 30

5.1 Variation Due to Change in Assumed Standard Deviation of Data 32

5.2 Variation Due to Change in Spherical Distance From the Center of Anomaly Block 35

5.3 Variation Due to Change in Time Interval of Data Points 36

5.4 Summary of Results 39

6. Prediction of 5° Equal Area Residual Anomalies 40

6.1 Variation Due to Change in Assumed Standard Deviation of Data 41

6.2 Variation Due to Change in Spherical Distance From the Center of Anomaly Block 41

6.3 Variation Due to Change in Time Interval of Data Points 44

6.4 Summary of Results 47

7. Effect of Uncertainty in Epoch Parameters on the Prediction of Anomalies 50

7.1 Effect on the Prediction of 10° Residual Anomalies ... 51

7.2 Effect on the Prediction of 5° Residual Anomalies 54

7.3 Interpretation of Results 56

8. Conclusions 58

References 60

0. Introduction

Our goal is the derivation of gravity anomalies at the surface of the earth from satellite to satellite range rates. The determination of gravity parameters from SST-observations is described in several reports, among others in (Schwarz, 1970; Kaula, 1972; Martin, 1972; Hajela, 1974a; Kaula et al, 1975). Common to the techniques described there is that the partial derivative of the sum range and range rate are formed with respect to the unknown parameters. From the partials a design matrix is built and the residual ranges and range rates (observed minus computed) are modeled in the least squares sense by the unknown parameters. Since implicitly in all methods of surface gravity parameter determination from satellite observations a downward continuation problem is involved, certain difficulties arise in the mentioned least squares methods. These difficulties are in keywords: truncation of the parameters to a "inner cap", stability of the solution, definition of resolution and so on. Therefore, Rummel (1975a, 1975b) proposed the method of least squares collocation for the stated problem. Least squares collocation should avoid the mentioned problems to a great extent. Since it will be split in different steps, each step can be separately checked for certain criteria such as *stability and resolution.*

In the sequel the method of determination of gravity anomalies by least squares collocation is described. The method will in a certain sense combine some ideas of Muller and Sjogren (1968), and of Kaula (1972) with least squares collocation.

In this report a theoretical procedure for recovery of gravity anomalies from SST data will be given in detail. The theory will then be examined through simulation studies that will demonstrate the accuracy of the proposed method and indicate the accuracy to be expected of the recovered anomalies.

1. Theoretical Discussion

We are considering satellite to satellite tracking (SST) observations in a "high-low" experiment such as between the ATS-6 and GEOS-3 satellites. The data gathered in a SST experiment are sum range and sum range rate, both types being described in (Martin, 1972; Hajela, 1974). Because of the low information content of sum range data for gravity parameter determination only sum range rate data will be analyzed in this study.

The observed sum range rate, $\dot{R}_{obs}$, is defined by:

$$(1.1) \qquad \dot{R}_{obs} = \tfrac{1}{2}\left(\dot{R}_{gru} + \dot{R}_{rcd} + \dot{R}_{rcu} + \dot{R}_{grd}\right)$$

with subscripts g, c, and r for ground tracking station, close satellite (e.g. GEOS-3), and relay satellite (e.g. ATS-6), and with subscripts u and d for measurements directed upwards and downwards.

Because the gravity field in the altitude of the relay satellite is highly attenuated, the range rates $\dot{R}_{gru}$ and $\dot{R}_{grd}$ may be computed very well from a low degree set of potential coefficients. Doing this, we find the mean range rate $\dot{R}_{rc}$ between the relay and the close satellite from:

$$(1.2) \qquad \dot{R}_{rc} = \tfrac{1}{2}\left(\dot{R}_{rcd} + \dot{R}_{rcu}\right) = \dot{R}_{obs} - \tfrac{1}{2}\left(\dot{R}_{gru} + \dot{R}_{grd}\right)$$

The time variation of $\dot{R}_{rc}$ is expressed by:

$$(1.3) \qquad \ddot{R}_{rc} = \frac{d\,\dot{R}_{rc}}{dt} \doteq \frac{\Delta\,\dot{R}_{rc}}{\Delta t}$$

The acceleration $\ddot{R}_{rc}$ is central for our computations and will now be discussed in more detail.

The orbit of the relay as well as of the close satellite is defined at every instant by their position vectors $\underline{X}$ and velocity vectors $\dot{\underline{X}}$. After applying corrections for side effects such as solar radiation pressure and atmospheric drag the acceleration vector $\ddot{\underline{X}}$ is:

$$(1.4) \qquad \ddot{\underline{X}} = \underline{\nabla V} \,,$$

where $\underline{\nabla V}$ is the gradient of the actual harmonic potential of the earth. The difference of the acceleration vector of the relay satellite, $\ddot{\underline{X}}_r$ and that of the close satellite, $\ddot{\underline{X}}_c$, yields:

$$(1.5) \qquad \ddot{\underline{X}}_{rc} = \underline{\nabla V}_r - \underline{\nabla V}_c$$

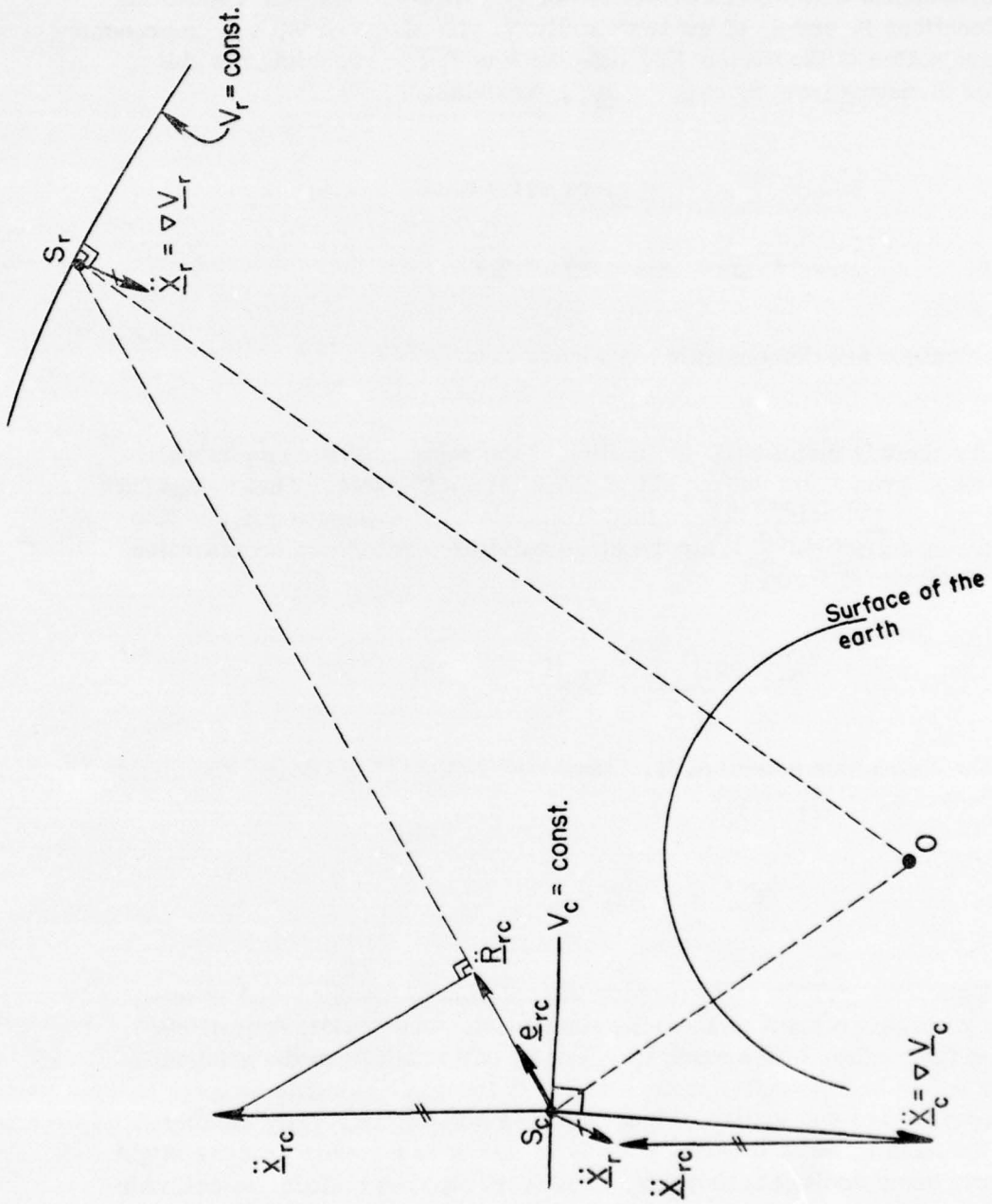

Figure 1.1 : Geometrical interpretation of the acceleration vectors in a SST experiment

The doppler instrumentation detects only the quantity $\dot{\dot{R}}_{rc}$ of equation (1.3), which is the magnitude of the vector $\underline{\dot{\dot{R}}}_{rc}$ in a straight line connecting the locations S_r and S_c of the two satellites. In other words, $\dot{\dot{R}}_{rc}$ represents the projection of the vector $\underline{\dot{\dot{X}}}_{rc}$ onto the line $\overline{S_r S_c}$. Denoting the unit vector directing from S_r to S_c by $\underline{e}_{rc}$, we obtain:

$$\dot{\dot{R}}_{rc} = \underline{\dot{\dot{X}}}_{rc} \cdot \underline{e}_{rc}, \text{ or using equation (1.5)}$$

$$\dot{R}_{rc} = \underline{\nabla V}_r \cdot \underline{e}_{rc} - \underline{\nabla V}_c \cdot \underline{e}_{rc} \tag{1.6}$$

These basics are demonstrated in Figure 1.1.

As already mentioned, the motion of the relay satellite can be well described from a low degree set of potential coefficients. That means that the gradient $\underline{\nabla V}_r$ can be determined from this set. Computing in addition a reference gradient $\underline{\nabla V}_c^{ref}$ for the close satellite a reference acceleration $\dot{\dot{R}}_{rc}^{ref}$ is obtained from:

$$\dot{\dot{R}}_{rc}^{ref} = \left(\underline{\nabla V}_r - \underline{\nabla V}_c^{ref}\right) \cdot \underline{e}_{rc}$$

With the anomalous potential, T, defined by $T = V - V^{ref}$ we derive the residual acceleration, $\dot{\dot{R}}_{rc}^{res}$, from:

$$\dot{\dot{R}}_{rc}^{res} = -\underline{\nabla T}_c \cdot \underline{e}_{rc} \tag{1.7}$$

Equations (1.1) to (1.7) provide the relation of the observed range rates with the gradient of anomalous potential. The gravity anomalies, Δg, on the surface of the earth may now be estimated from the gradient of the anomalous potential at the altitude of the close satellite by a straightforward application of least squares collocation. Only the fact that the input quantity to collocation is in this case a vector process might deserve some additional thoughts. The least squares collocation estimate of Δg at any point Q on the surface of the earth is (Rummel, 1975a):

$$(1.8)\qquad \hat{\Delta g}(Q) = \underset{1\cdot 1}{\underline{C}(Q)_{\Delta g\,\nabla T_j}}\ \underset{1\cdot 3n}{(\underline{\underline{C}}_{\nabla T_j \nabla T_i}}\ \underset{3n\cdot 3n}{+\ \underline{\underline{D}}_{ji}}\underset{3n\cdot 3n}{)^{-1}}\ \underset{3n\cdot 1}{\underline{\nabla T_i}}$$

with $\underline{C}(Q)_{\Delta g\,\nabla T_j}$ .... crosscovariance vector between $\Delta g(Q)$ and the input elements $\underline{\nabla T}_j$ at the points P, j=1, ...n, dim (1·3n),

$\underline{\underline{C}}_{\nabla T_j \nabla T_i}$ ..... matrix of the autocovariances between the anomalous potential gradients $\underline{\nabla T}_j$ with dim (3n·3n),

$\underline{\underline{D}}_{ji}$ ..... noise matrix

What we would need to apply this equation to anomaly recovery is the vector of gradients $\underline{\nabla T}_i$. But actually we have only $\ddot{R}_{rc}^{res}$, the projection of the gradient onto the line connecting the close and the relay satellite as expressed in equation (1.7). In other words we would like to find the inverse of this projection, that means an expression of the form:

$$\underline{\nabla T}_c = \underline{A}\,\ddot{R}_{rc}^{res}$$

In order to define the projector $\underline{A}$ one would have to know not only the direction defined by $\underline{e}_{rc}$ but also the direction of the gradient $\underline{\nabla T}_c$, with unit vector, $\underline{e}_{\nabla T}$, which is not available to us. The problem becomes obvious by going back to equation (1.7): Rewritting equation (1.7) in components of a rotating (X_1, X_2, X_3) coordinate system we obtain

$$\ddot{R}_{rc}^{res} = -\left(\frac{\partial T_c}{\partial X_1}\,\underline{e}^{X_1} \cdot \underline{e}_{rc}^{X_1} + \frac{\partial T_c}{\partial X_2}\,\underline{e}^{X_2} \cdot \underline{e}_{rc}^{X_2} + \frac{\partial T_c}{\partial X_3}\,\underline{e}^{X_3} \cdot \underline{e}_{rc}^{X_3}\right)$$

This equation contains the three unknowns, $\frac{\partial T_c}{\partial X_i}$, $i = 1, 2, 3$, which means that we need at least three linearly independent equations of this type at every instant in order to be able to determine the gradient $\underline{\nabla T}_c$. As a result we note:

> For a unique recovery of gravity quantities from a "high-low" SST experiment at least three relay satellites are needed that track the close satellite simultaneously.

Instead of postulating this ideal situation we will assume the more realistic case of only a satellite pair. From the above result it becomes obvious that a certain approximation has to be introduced at this point. Basically we may choose between two types of approximations, both with respect to the direction of the gradient, $\underline{\nabla T}_c$.

Approximation (I):

$$\underline{\nabla T_c} \doteq \left(\frac{\partial T}{\partial r} , 0 , 0 \right)^T \quad \left((.)^T \ldots \text{transposed} \right) \tag{1.9}$$

which means the gradient of the anomalous potential has approximately only a radial component.

Approximation (II):

$$\underline{\nabla T_c} \doteq \frac{|\underline{\nabla T_c}|}{|\underline{\nabla V_c^{ref}}|} \underline{\nabla V_c^{ref}} , \tag{1.10}$$

which means the gradient $\underline{\nabla T_c}$ has approximately the direction of ∇V_c^{ref}. The geometrical interpretation for both approximations is given in Fig. 1.2.

We expect that by using approximation (II) a smaller error is committed than by using approximation (I). But this advantage has to be paid by a far higher computational effort since (1) for each observational point $\underline{\nabla V_c^{ref}}$ has to be computed and (2) multivariate collocation has to be used as expressed by equation (1.8).

Since we are convinced that approximation (I) is for most practical situations sufficient we continue to analyze only the latter. Assuming equation (1.9) to be valid the relation to the acceleration $\ddot{R}_{rc}^{res}$ is:

$$\underline{\nabla T_c} \doteq \left(\frac{\partial T}{\partial r} , 0 , 0 \right)^T = \frac{\ddot{R}_{rc}^{res}}{\cos\beta} \underline{e_c}$$

where β is the spatial angle between the vectors $\underline{\nabla T_c}$ and $\underline{\ddot{R}_{rc}^{res}}$ with $\cos\beta = \underline{e_c} \cdot \underline{e_{rc}}$, with $\underline{e_c}$ the unit vector in the radial direction at the close satellite.

Using only the radial component this equation becomes:

$$T_r = \frac{\partial T}{\partial r} = \frac{\ddot{R}_{rc}^{res}}{\cos\beta} \tag{1.11}$$

From equation (1.11) it follows that errors, $\epsilon_{\ddot{R}}$, in $\ddot{R}_{rc}^{res}$ propagate to errors $\epsilon_{\frac{\partial T}{\partial r}}$ in $\frac{\partial T}{\partial r}$ by

$$\text{var}\left(\epsilon_{\frac{\partial T}{\partial r}} \right) = \frac{1}{\cos^2\beta} \text{var}\left(\epsilon_{\ddot{R}} \right) \tag{1.12}$$

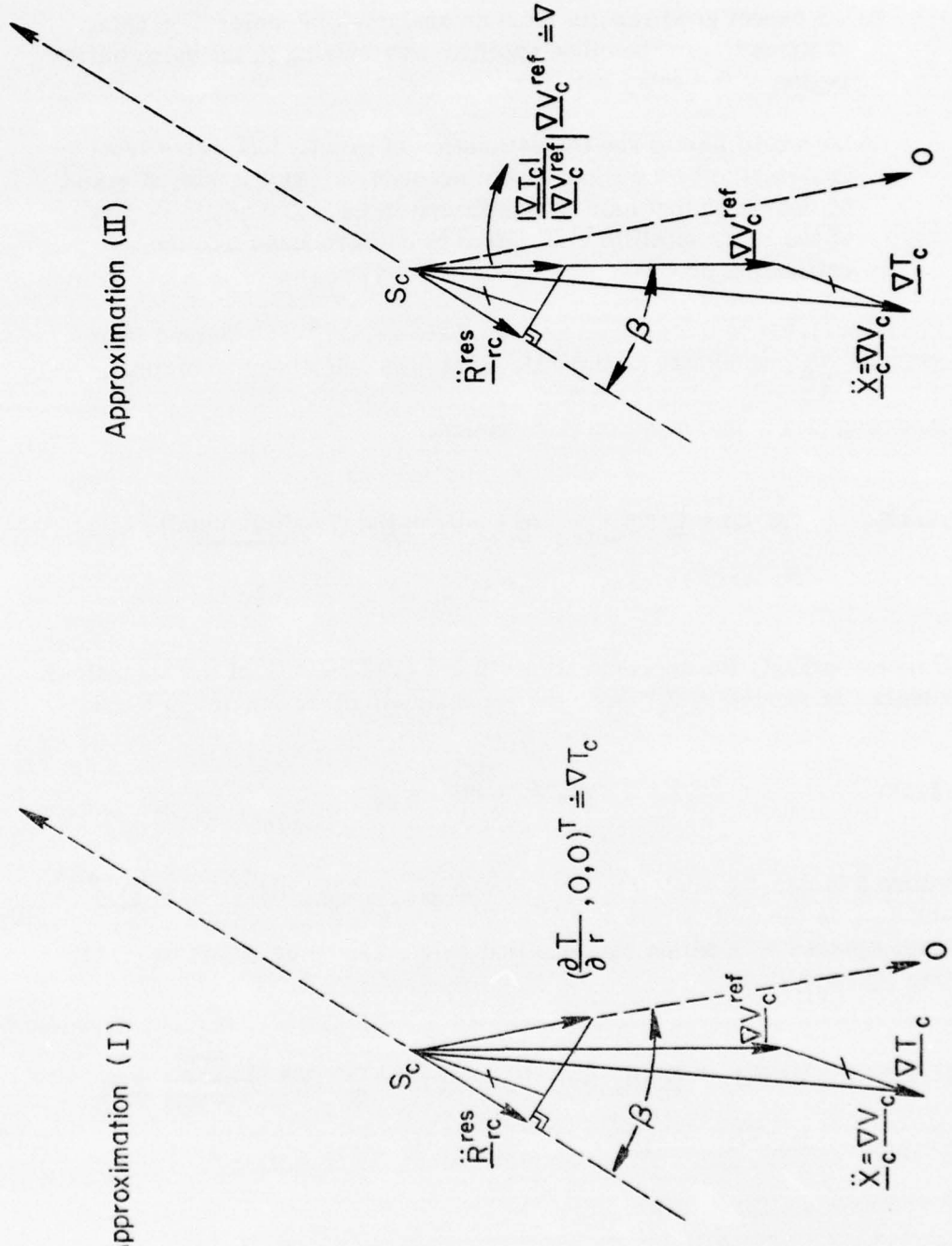

Figure 1.2 : Geometrical principle of approximations (I) and (II)

This relation demonstrates the importance of the geometry of the relay to the close satellite on the errors. From (1.12) follows:

(1) We expect good results from an analysis of acceleration data at times where the close satellite was moving in the subsatellite region of the relay satellite.

(2) We would like to see the estimation of gravity quantities from SST-data to be an almost local procedure. This means it would be desirable that only data gathered in the subsatellite region of the relay satellite would have to be introduced into the estimation process.

Equation (1.11) is the desired relation between $\ddot{R}_{rc}^{res}$ as obtained from SST and $\frac{\partial T}{\partial r}$ which can be introduced into the collocation solution.
Inserting (1.11) into equation (1.8) yields:

$$\hat{\Delta g}(Q) = \underset{1\cdot n}{\underline{C}(Q)_{\Delta g\, Tr\, j}} \; \underset{n\cdot n}{(\underline{\underline{C}}_{Tr\, j\, Tr\, i} + \underline{\underline{D}}_{ji})^{-1}} \; \underset{n\cdot 1}{(\underline{\ddot{R}_{rc}^{res}/\cos\beta})_i} \qquad (1.13)$$

dim: $1\cdot 1$ $\quad 1\cdot n$ $\quad n\cdot n$ $\quad n\cdot n$ $\quad n\cdot 1$

Correspondingly for approximation (II) the gradient $\underline{\nabla T_c}$ of the anomalous potential is related to $\ddot{R}_{rc}^{res}$ with the approximate direction of $\underline{\nabla V_c^{ref}}$ by:

$$\underline{\nabla T_c} \doteq \frac{\ddot{R}_{rc}^{res}}{\cos\beta}\; \underline{e}_{\nabla V} \;, \qquad (1.14)$$

where β is now the spatial angle between $\underline{e}_{r_c}$ and the direction of $\underline{\nabla V_c^{ref}}$ and $\underline{e}_{\nabla V}$ is the unit vector of $\underline{\nabla V_c^{ref}}$. We obtain for the multivariate least squares collocation equation that solves for Δg by inserting (1.14) into equation (1.8)

$$\hat{\Delta g}(Q) = \underset{1\cdot n}{\underline{C}(Q)_{\Delta g\, \nabla V\, j}} \; \underset{3n\cdot 3n}{(\underline{\underline{C}}_{\nabla V\, j\, \nabla V\, i} + \underline{\underline{D}}_{ji})^{-1}} \; \underset{3n\cdot 1}{\left(\frac{\ddot{R}_{rc}^{res}}{\cos\beta}\; \underline{e}_{\nabla V}\right)_i} \qquad (1.15)$$

dim: $1\cdot 1$ $\quad 1\cdot n$ $\quad 3n\cdot 3n$ $\quad 3n\cdot 3n$ $\quad 3n\cdot 1$

Computational Procedure

The information provided to the user in a SST experiment is usually the time of measurement, the sum range and sum range rate observation, R_{obs} and $\dot{R}_{obs}$, respectively, as well as the orbital elements at certain periods of time. Using the GEODYN (Martin, 1972) program we can compute the range rate, $\dot{R}_{comp}$, at the times of measurement from a set of potential coefficients and the given orbital elements. The difference between observed and computed range rate is:

$$\dot{R}_{rc}^{res} = \dot{R}_{obs} - \dot{R}_{comp} , \tag{1.16}$$

which is the relative velocity between the close and the relay satellite in the line connecting the two satellites. As indicated in equation (1.3) we have then to find the acceleration $\ddot{R}_{rc}^{res}$. The necessary numerical differentiation may be critical for the whole processing and therefore deserves special attention.

We propose three different types of numerical differentiation. Even though their features might be analyzed theoretically, only their application on real data will give a final answer what procedure should be chosen. The first two methods of numerical differentiation are deterministic. This is to a certain extent a drawback because the range rate data will be disturbed by observational errors. But after filtering the raw data these procedures should also be applicable with advantage.

(1) Finite Differences: (e.g. Whittaker and Robinson, 1967, p. 62) It is assumed that the residual range rates, $\dot{R}_{rc}^{res}$, are given free of noise equidistant with time in intervals of w. Then, we find

$$\ddot{R}_{rc}^{res}(t_o) = \frac{1}{w}\left[\Delta \dot{R}_{rc}^{res}(t_o) - \frac{1}{2}\Delta^2 \dot{R}_{rc}^{res}(t_o) + \frac{1}{3}\Delta^3 \dot{R}_{rc}^{res}(t_o) - \frac{1}{4}\Delta^4 \dot{R}_{rc}^{res}(t_o)\ldots\right],$$

where Δ, Δ^2, Δ^3, Δ^4 are the first to fourth differences obtained from the data in a difference scheme. Thus, from each sequence of, for example six, non overlapping--data an estimate for $\ddot{R}_{rc}^{res}$ can be determined.

(2) Spline Method: (e.g. Shampine and Allen, 1973, p. 54)
This method seemed more accurate to us than method (1) and was therefore used in the simulation.

A cubic interpolatory spline is computed for each sequence of five or more--non overlapping--$\dot{R}^{res}_{r\,c}$ data by a program given in (ibid). By a minor modification of this FORTRAN program the derivative $\ddot{R}^{res}_{r\,c}$ is obtained at any desired point inside the used data interval. For details, see Section 4.3.

(3) Least Squares Collocation:
The advantage of least squares collocation would be that in contrast to methods (1) and (2) the filtering of observational noise can be implemented into the procedure.

Using the classical least squares prediction formula

$$\hat{R}^{res}_{r\,c}(t) = \underline{C}(t)_{t\,i}\,(\underline{\underline{C}}_{t\,i\,t\,j} + \underline{\underline{D}}_{t\,i\,t\,j})^{-1}\;\underline{\dot{R}}^{res}_{r\,c,\,t\,j} \tag{1.17}$$

we obtain from the vector of residual range rates an approximation to the range rate function $\hat{\dot{R}}^{res}_{r\,c}(t)$ at any desired point on the real (time-) line. The quantities appearing in equation (1.17) are:
$\underline{C}(t)_{t\,i}$ ... the autocovariance vector between the observations and the prediction point,
$\underline{\underline{C}}_{t\,i\,t\,j}$ ... the autocovariance matrix of the observations, and

$\underline{\underline{D}}_{t\,i\,t\,j}$ ... the observational noise matrix.
The autocovariance function C(t) of $\dot{R}^{res}_{r\,c}$ can be determined by approximating to an empirical covariance sequence--as derived from simulated noise free data--a positive semidefinite function such as a Gaussian, second-order Markov, or third-order Markov model shown in (Jordan, 1972). The autocovariance function C(t) + D(t) can be derived in the same way using real data. From these two functions, C(t) and C(t) + D(t) the covariance vector and matrix needed in equation (1.17) can be built.

The acceleration, $\hat{\ddot{R}}^{res}_{r\,c}$, is now computed at any desired point on the real line by differentiating equation (1.17),

$$\hat{\ddot{R}}^{res}_{r\,c}(t) = \left(\frac{\partial C(t)}{\partial t}\right)_{t\,i}\left(\underline{\underline{C}}_{t\,i\,t\,j} + \underline{\underline{D}}_{t\,i\,t\,j}\right)^{-1}\underline{\dot{R}}^{res}_{r\,c,\,t\,j} \tag{1.18}$$

Since the differentiation is directly carried out on the analytical expression for C (t) equation (1.18) can be interpreted as an analytical differentiation of the approximate function, $\dot{R}^{res}_{rc}(t)$, derived from (1.16).

The solution proposed and applied by Muller and Sjogren (1968) for the lunar experiment is of type (2).

After computing $\ddot{R}^{res}_{rc}$, $\cos\beta$ has also to be determined. For approximation (I) we have $\cos\beta = \underline{e}_c \cdot \underline{e}_{rc}$ where $\underline{e}_{rc}$ is computed from the geocentric coordinates of the relay and the close satellite and $\underline{e}_c$ from the geocentric coordinates of only the close satellite. The geocentric coordinates are provided by the GEODYN program together with the computed range rates.

More tedious is the computation of $\cos\beta$ using approximation (II). Then we use $\cos\beta = \underline{e}_{\nabla V} \cdot \underline{e}_{rc}$ and the unit vector $\underline{e}_{\nabla V}$ for the gradient of the reference potential, $\underline{\nabla V}^{ref}_c$ has to be determined for each instant from the set of potential coefficients.

Finally, least squares collocation in form of equations (1.13) or (1.15) is applied on the approximate values for $\underline{\nabla T}_c$ derived from equations (1.11) or (1.14). The covariance elements will be computed from global covariance expressions such as those derived in (Tscherning and Rapp, 1974). Thereby we use the FORTRAN programs developed by Tschering (1976) which provide the covariance of the anomalous potential, the gravity anomaly and their first and second derivatives. The estimated gravity anomalies are chosen to be located on a sphere whose center is at the earth's center of mass and with the mean radius of the earth. Mean anomalies are computed by numerical integration of the appropriate covariances.

The problem of determining gravity anomalies at the surface of the earth from $\frac{\partial T}{\partial r}$ values in satellite altitude lies in the fact that a downward continuation has to be carried out. This will give us two types of difficulties: (1) Small errors at satellite altitude will blow up to large errors in Δg after the downward continuation operation is applied on them. (2) The downward continuation operation may cause severe stability problems.

To get an idea about this operation the expression $\underline{C}(Q)_{\Delta g\, r_j} (\underline{\underline{C}}_{r_i\, r_j} + \underline{\underline{D}})^{-1}$ of equation (1.13) has been computed for a point, and a 10° equal area block that is to be estimated. The above covariance expression transforms the $(\ddot{R}^{res}_{rc} / \cos\beta)$-values to Δg - values at the surface of the earth. The given data are assumed to have a spherical

distance of 0° to 90° in 5° steps from the center of the surface Δg-block and are located in 250 km altitude. The noise is considered to be zero. The results are given in Figure 1.3, where the values of a vector $\underline{A} = \underline{C}\ (O)_{\Delta g \Delta r\, j}\ \underline{\underline{C}}^{-1}_{\Delta r\, j \Delta r\, i}$ are presented with increasing spherical distance from the estimation point. Even though we know that theoretically we would have to have given the $\frac{\partial T}{\partial r}$ values as a continuous function on a sphere concentric with the center of the earth and in satellite altitude, Figure 1.3 shows that for our practical situation data have only to be given up to a maximum spherical distance of about 20° from the estimation point. For a spherical distance of 10° the influence of the data is already below 20% of the influence of the data with 0° spherical distance. This question will be analyzed further in detail in the simulation study. In the simulation only approximation (I) will be considered.

2. The Covariance Functions

The evaluation of (1.13) requires, in part, the determination of the covariances between the $\frac{\partial T}{\partial r}$ values at points i and j, and the covariance between the anomaly being predicted and the observed or given $\frac{\partial T}{\partial r}$ value. Such covariance functions can be derived in an analytical way using an assumed model for the anomaly degree variances (Tscherning and Rapp, 1974, Tscherning, 1976). In the Tscherning (1976) discussion covariances were computed for gravity anomalies, $\frac{-\partial T}{\partial r}\Big/ r$ and other quantities not of specific interest for this report. We let:

$$A \equiv \frac{-1}{r}\ \frac{\partial T}{\partial r} \quad \text{or} \quad \frac{\partial T}{\partial r} = -rA \tag{2.1}$$

Then the covariance between the $\frac{\partial T}{\partial r}$ values is:

$$\operatorname{cov}\left(\frac{\partial T}{\partial r}\Big|_P\ \frac{\partial T}{\partial r}\Big|_Q\right) = M\left\{(-r_P A_P)(-r_Q A_Q)\right\} \tag{2.2}$$

$$= r_P r_Q \operatorname{cov}(A_P A_Q)$$

Here M indicates an average value over the earth and r is the distance from the center of the earth to the point in question.

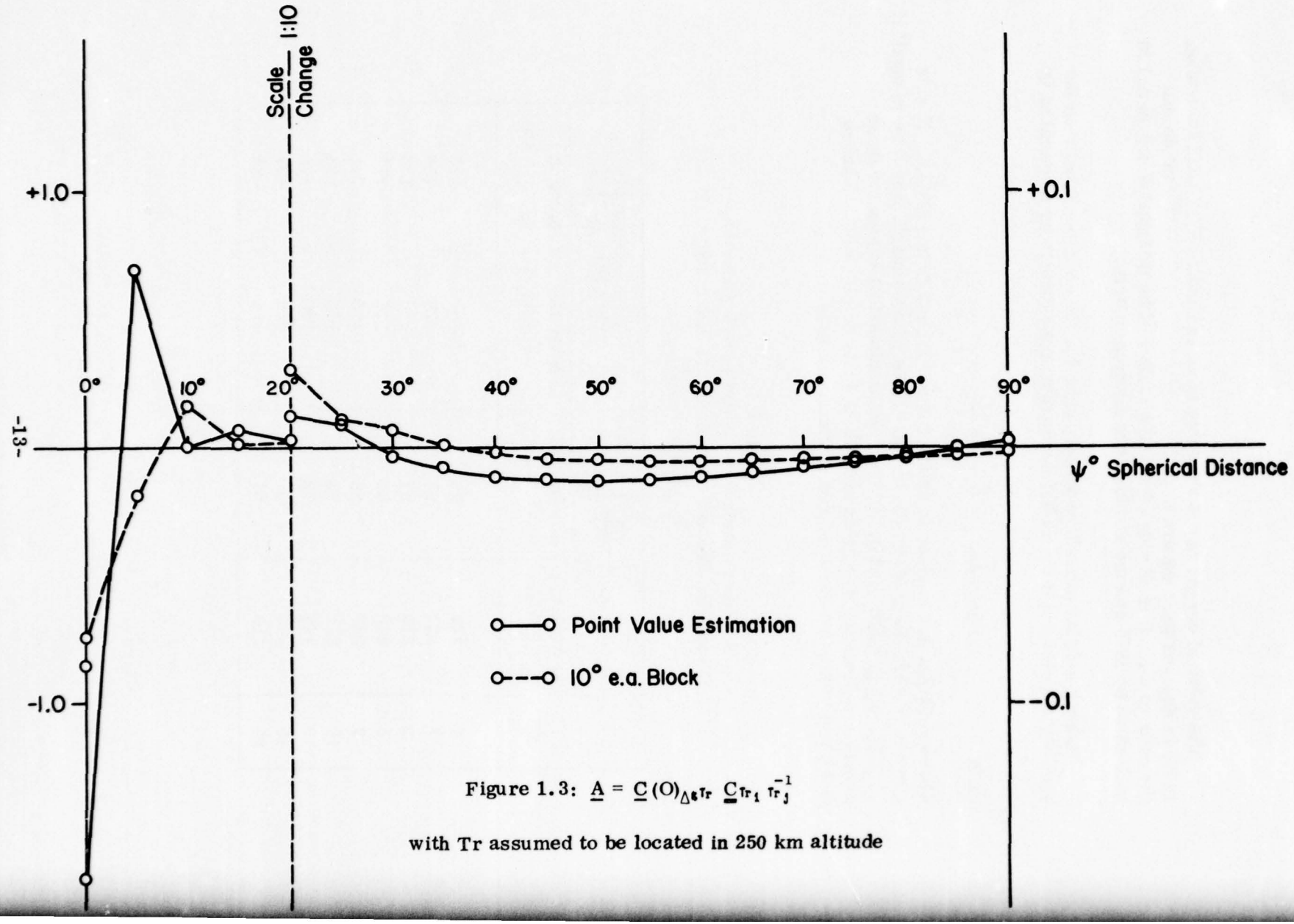

Figure 1.3: $\underline{A} = \underline{C}(O)_{\Delta g_{Tr}} \underline{C}_{Tr_i Tr_j}^{-1}$

with Tr assumed to be located in 250 km altitude

The value of $\mathrm{cov}(A_P\ A_Q)$ is available from subroutine COVAX (Tscherning, 1976) in Eotovos units squared. $1E^2$ is equal to 1×10^{-8} mgal^2/m^2 so that the units of the left hand side of equation (2.2) will be in mgal^2 if $\mathrm{cov}(A_P\ A_Q)$ is multiplied by 10^{-8} and the r values are given in meters.

Using a similar procedure we can write for the covariance between the anomaly at point P and the radial derivative of the disturbing potential at Q:

$$\mathrm{cov}\left(\Delta g_P\ ,\ \frac{\partial T}{\partial r}\Big|_Q\right) = -r_Q\ \mathrm{cov}(\Delta g_P\ A_Q) \tag{2.3}$$

where $\mathrm{cov}(\Delta g_P\ A_Q)$ is given in units of mgal $\cdot$ E units from COVAX. If r is given in meters the units on the left hand side of equation (2.3) will be in mgal^2 if $\mathrm{cov}(\Delta g_P\ A_Q)$ is multiplied by 10^{-4}. Typical numerical values for these covariance functions are given in Table 2.1 (for an ellipsoid reference field) and Table 2.2 (for a degree 12 reference field).

Table 2.1
Sample Covariances Needed in SST Reduction
Given With Respect to an Ellipsoid Reference Field
(Units: mgal^2)

	$\mathrm{cov}\left(\frac{\partial T}{\partial r}\Big|_P\ \frac{\partial T}{\partial r}\Big|_Q\right)$		$\mathrm{cov}\left(\Delta g_P\ \frac{\partial T}{\partial r}\Big|_Q\right)$	
ψ °	h_P = 250 km h_Q = 250 km	h_P = 850 km h_Q = 850 km	h_P = 0 m h_Q = 250 km	h_P = 0 m h_Q = 850 km
0	327	98	-341	-128
1	324	97	-329	-128
2	316	97	-300	-125
5	276	93	-216	-112
7	247	89	-176	-101
10	208	82	-134	-84
13	175	73	-103	-68
15	154	67	-86	-59
20	110	51	-54	-39

Table 2.2
Sample Covariances Needed in SST Reduction
Given With Respect to a Degree 12 Reference Field
(Units: $mgal^2$)

	$cov\left(\frac{\partial T}{\partial r}\Big\|_P \frac{\partial T}{\partial r}\Big\|_Q\right)$		$cov\left(\Delta g_P \frac{\partial T}{\partial r}\Big\|_Q\right)$	
ψ°	$h_P = 250$ km $h_Q = 250$ km	$h_P = 850$ km $h_Q = 850$ km	$h_P = 0$ m $h_Q = 250$ km	$h_P = 0$ m $h_Q = 850$ km
0	50	1.53	-129	-15
1	47	1.51	-117	-15
2	41	1.41	-91	-13
5	15	0.84	-21	-6
7	2	0.36	3	-1
10	-9	-0.30	16	3
13	-9	-0.48	15	4
15	-7	-0.46	10	3
20	1	-0.06	-2	-0

Examination of the values given in Tables 2.1 and 2.2 show the rapid decrease in correlation as the altitude increases from 250 km to 850 km. This decrease is simply a numerical representation of the attentuation of the anomalous gravity field with height. We also note that the covariances with respect to the ellipsoidal field change very slowly decreasing to the first zero crossing for the radial derivative autocovariances at $\psi = 38^\circ$ (for both altitudes) and for the covariance between the surface anomaly and the radial derivative at $\psi = 34^\circ$ (for both altitudes). When the higher degree surface is used as reference the magnitude of the covariances considerably decreases and the first zero crossings occur at smaller ψ values. This would indicate that only data close to the computation area can be used when the higher degree reference surface is used. This statement will be examined in the simulation studies to be discussed in the next sections of this report.

3. Preliminary Simulation Studies

Before extensive simulation studies are performed it is of interest to investigate the accuracy to be expected in the recovery of gravity anomalies from $\partial T/\partial r$ values. Using the notation of equation (1.13) the error variance of the estimated gravity anomaly is :

$$(3.1) \qquad m^2\left(\hat{\Delta g}(Q)\right) = C(\Delta g) - \underline{C}(Q)_{\Delta g T_r j}\left(\underline{\underline{C}}_{T_r j T_r i} + \underline{\underline{D}}_{ji}\right)^{-1} \underline{C}'(Q)_{\Delta g T_r j}$$

where m is the standard deviation of the prediction and $C(\Delta g)$ is the variance (or mean square value) of the anomaly block being estimated. Since we are dealing with mean anomalies, all covariances dealing with Δg values have been computed by numerical integration of the point covariance functions over the mean anomaly block.

For this initial test, predictions were made for a 5° equal area block, and a $2^\circ \times 2^\circ$ block. A grid of 8 assumed data points surrounding the blocks to be predicted was established as is shown in Figure 3.1. The predictions were carried out for two assumed observation heights (250 km and 850 km) and for several accuracy specifications on the $\partial T/\partial r$ values.

The predicted accuracies, with respect to an ellipsoidal reference model, is given in Table 3.1 for the 5° block and Table 3.2 for the $2^\circ \times 2^\circ$ block.

Table 3.1
Accuracy of the Predicted 5° Anomaly Block
Using Known Data as Shown in Figure 3.1

Data Acc	Observation Height 250 km	850 km
0.0 mgals	3.6 mgals	3.1 mgals
0.1	3.6	5.3
1.0	4.0	8.1
2.0	4.8	10.2

Table 3.2
Accuracy of the Predicted $2^\circ \times 2^\circ$ Anomaly Block
Using Known Data as Shown in Figure 3.1

Data Acc	Observation Height 250 km	850 km
0.0 mgals	6.3 mgals	8.9 mgals
0.1	6.4	14.6
1.0	9.6	17.8
2.0	12.0	18.8

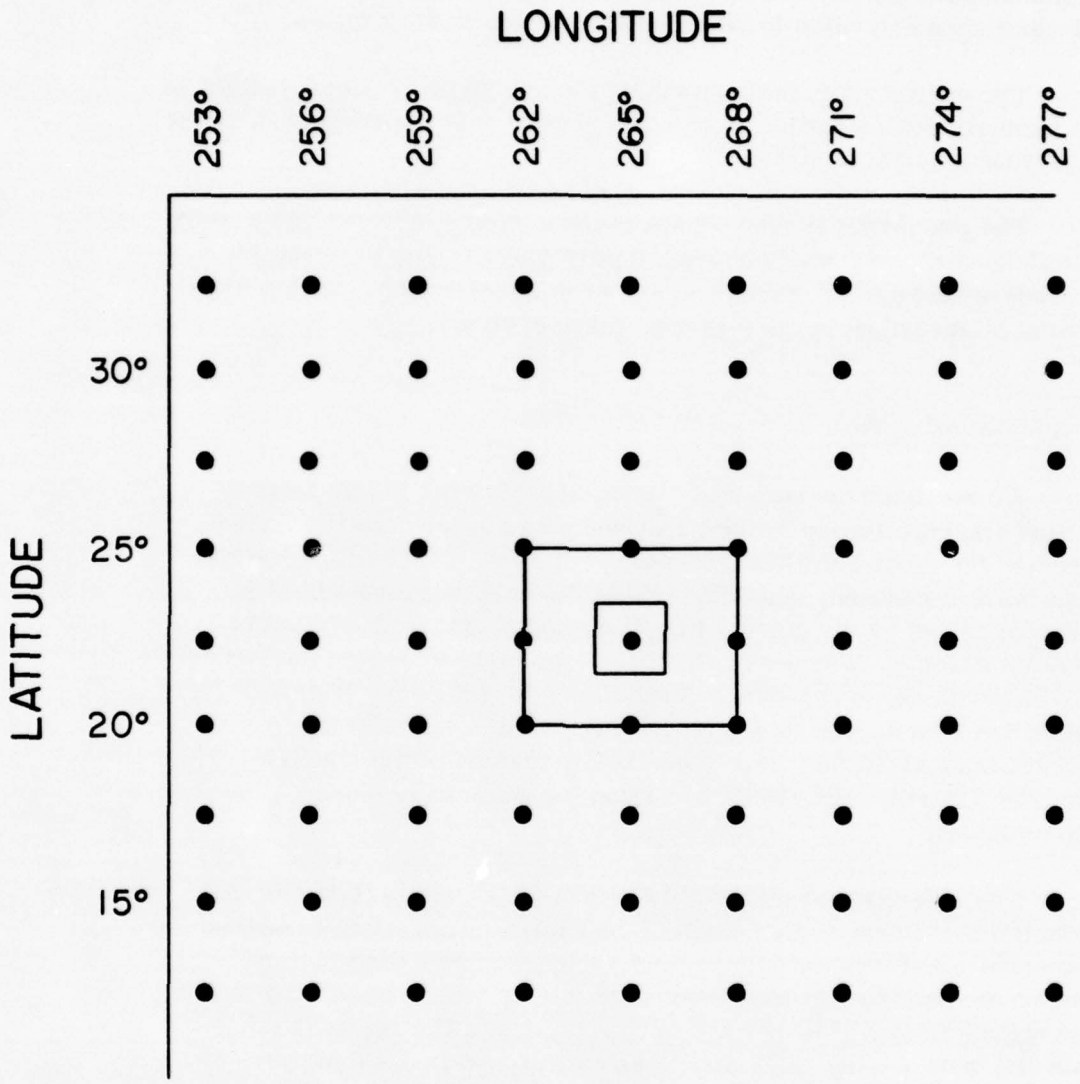

Figure 3.1: Location of 5° and 2° Anomaly Blocks To Be Predicted From Given $\frac{\partial T}{\partial r}$ Values at Indicated Points (•)

In judging the accuracy of figures given in Tables 3.1 and 3.2, it is helpful to note that the root mean 5° anomaly is about 18.9 mgals while the corresponding value for the $2^\circ \times 2^\circ$ anomaly is 25.2 mgals.

The values given in these tables clearly show the improvement in the anomaly determination as the data accuracy is improved and/or the observation height is reduced.

The promising results shown in these tables indicate that a more complete simulation study should be performed trying to formulate a procedure that closely relates to a real world situation. Such a simulation is described in the following three sections.

4. Simulation of Data

We consider the sum range rate, $\dot{R}_s$ (Martin, 1972), from a ground tracking station to the geosynchronous relay satellite ATS-6 tracking the close satellite GEOS-3. The $\dot{R}_s$ observations were simulated, considering that the earth's gravity field is fully described by the potential coefficients of the Goddard Earth Model 8 (GEM 8) (Wagner et al, 1975), complete to degree and order 25 along with some resonance coefficients to (30, 28). This will be called the high degree or the (30, 28) P.C. field, and the $\dot{R}_s$ observations as $\dot{R}_s(30, 28)$. The 7508.0 version of the GEODYN program (Martin et al, 1975) was used for generating these observations.

The reference gravity field for describing the earth's normal potential was taken as the potential coefficients, complete to degree and order 12, from the GEM 8 field. This will be called the low degree or the (12, 12) P.C. field, and the $\dot{R}_s$ values generated in this low degree field will be termed as $\dot{R}_s(12, 12)$. The residual range rate $\dot{R}_{rc}$ between the relay and close satellites was obtained as:

$$\dot{R}_{rc} = \dot{R}_s(30, 28) - \dot{R}_s(12, 12) \tag{4.1}$$

considering that the relay satellite is not perturbed over short periods by the potential coefficients higher than the low degree field.

The residual acceleration $\ddot{R}_{rc}$ between the relay and close satellites was obtained by the numerical differentiation of $\dot{R}_{rc}$ values. This was done by fitting a natural cubic interpolatory spline to $\dot{R}_{rc}$ values. The details of the procedure will be described later in Section 4.3.

In judging the accuracy of figures given in Tables 3.1 and 3.2, it is helpful to note that the root mean 5° anomaly is about 18.9 mgals while the corresponding value for the $2^\circ \times 2^\circ$ anomaly is 25.2 mgals.

The values given in these tables clearly show the improvement in the anomaly determination as the data accuracy is improved and/or the observation height is reduced.

The promising results shown in these tables indicate that a more complete simulation study should be performed trying to formulate a procedure that closely relates to a real world situation. Such a simulation is described in the following three sections.

4. Simulation of Data

We consider the sum range rate, $\dot{R}_s$ (Martin, 1972), from a ground tracking station to the geosynchronous relay satellite ATS-6 tracking the close satellite GEOS-3. The $\dot{R}_s$ observations were simulated, considering that the earth's gravity field is fully described by the potential coefficients of the Goddard Earth Model 8 (GEM 8) (Wagner et al, 1975), complete to degree and order 25 along with some resonance coefficients to (30, 28). This will be called the high degree or the (30, 28) P.C. field, and the $\dot{R}_s$ observations as $\dot{R}_s(30, 28)$. The 7508.0 version of the GEODYN program (Martin et al, 1975) was used for generating these observations.

The reference gravity field for describing the earth's normal potential was taken as the potential coefficients, complete to degree and order 12, from the GEM 8 field. This will be called the low degree or the (12, 12) P.C. field, and the $\dot{R}_s$ values generated in this low degree field will be termed as $\dot{R}_s(12, 12)$. The residual range rate $\dot{R}_{rc}$ between the relay and close satellites was obtained as:

$$\dot{R}_{rc} = \dot{R}_s(30, 28) - \dot{R}_s(12, 12) \tag{4.1}$$

considering that the relay satellite is not perturbed over short periods by the potential coefficients higher than the low degree field.

The residual acceleration $\ddot{R}_{rc}$ between the relay and close satellites was obtained by the numerical differentiation of $\dot{R}_{rc}$ values. This was done by fitting a natural cubic interpolatory spline to $\dot{R}_{rc}$ values. The details of the procedure will be described later in Section 4.3.

The inertial position and velocity vectors, and the latitude, longitude and height above the ellipsoid, of the relay and close satellites were also generated in the low degree field using the Geodyn program. If at time t, the inertial position coordinates of the relay and close satellites are given by X_r, Y_r, Z_r, X_c, Y_c, Z_c respectively, then the position vectors $\underline{r}_r$, $\underline{r}_c$ of the relay and close satellites, and the respective unit position vectors $\underline{e}_r$ and $\underline{e}_c$, as well as the position vector $\underline{r}_{rc}$ from the relay to close satellite, may be computed from:

$$(4.2) \qquad \underline{e}_r = \underline{r}_r / |\underline{r}_r| = (X_r \underline{i} + Y_r \underline{j} + Z_r \underline{k}) / (X_r^2 + Y_r^2 + Z_r^2)^{1/2}$$

$$\underline{e}_c = \underline{r}_c / |\underline{r}_c| = (X_c \underline{i} + Y_c \underline{j} + Z_c \underline{k}) / (X_c^2 + Y_c^2 + Z_c^2)^{1/2}$$

$$\underline{e}_{rc} = \underline{r}_{rc} / |\underline{r}_{rc}| = \left((X_c - X_r) \underline{i} + (Y_c - Y_r) \underline{j} + (Z_c - Z_r) \underline{k}\right) / \left((X_c - X_r)^2 + (Y_c - Y_r)^2 + (Z_c - Z_r)^2\right)^{1/2}$$

with usual notations for the magnitude of a vector, and the unit coordinate vectors.

The angle β between the radial direction at the close satellite, and the direction from the close satellite to the relay satellite may then be computed from:

$$(4.3) \qquad \cos\beta = (-\underline{e}_c) \cdot (-\underline{e}_{rc}) = \underline{e}_c \cdot \underline{e}_{rc}$$

$$= \left(X_c (X_c - X_r) + Y_c (Y_c - Y_r) + Z_c (Z_c - Z_r)\right) / |\underline{r}_c| |\underline{r}_{rc}|$$

The anomalous potential T with respect to the low degree field is then, using approximation (I), related to $\ddot{R}_{rc}$ values through the relation:

$$(4.4) \qquad (\partial T / \partial r)_c \doteq \ddot{R}_{rc} / \cos\beta$$

The residual gravity anomalies $\underline{\Delta g}'$ referred to the low degree field may then be predicted as discussed in Section 3. The data required for these computations are the latitude φ_c, longitude λ_c, height h_c of the close satellite along with $(\partial T / \partial r)_c$ at the close satellite at various times.

Further details about the generation of this data are described in this section.

4.1 Residual 10° and 5° Equal Area Mean Anomalies

The potential coefficients in the GEM 8 field are referred to the following values of the gravitational constant times the mass of the earth kM, the semi-major axis a_e of the ellipsoid, and the fully normalized potential coefficient of degree 2 order 0, $\bar{C}_{2,0}$ as:

(4.5)
$$kM = 3 \cdot 986,008 \times 10^{14} \ m^3/sec^2$$
$$a_e = 6,378,145 \ m$$
$$\bar{C}_{2,0} = -484 \cdot 164,57 \times 10^{-6}$$

The flattening f of the ellipsoid may be computed (Hajela, 1974b, page 7) by iteration from:

$$(4.6) \qquad f = \left[\frac{3}{2} J_2 + \frac{\omega^2 a^3 (1-f)}{2kM} \left(1 - \frac{2}{7} f + \frac{11}{49} f^2 + \ldots \right) \right] \Big/ \left(1 - \frac{f}{2} \right),$$

where ω is the rotational velocity of the earth, and the dynamical form factor J_2 is given by:

$$J_2 = -\sqrt{5} \ \bar{C}_{2,0}$$

resulting in the value of flattening as:

(4.7)
$$f = 1/298 \cdot 257$$

The mean gravity anomaly Δg_{PC} of a block, bounded by geocentric latitudes φ_N', φ_S' and longitudes λ_E, λ_W, as implied by the potential coefficients up to degree N_{MAX} is given, after neglecting the zero degree value of the gravity anomaly, by (Desrochers, 1971, page 13):

$$(4.8) \qquad \Delta g_{PC} = \frac{kM/r^2}{\Delta\lambda(\sin\varphi_N' - \sin\varphi_S')} \sum_{N=2}^{N_{MAX}} (n-1) \left(\frac{a_e}{r} \right)^n \left[\Delta\lambda \ \bar{C}_{N,0}^* \int_{\varphi_S'}^{\varphi_N'} \bar{P}_{N,0} \right.$$

$$(\sin\varphi') \ \cos\varphi' \, d\varphi' + \sum_{M=1}^{N} \frac{1}{m} \left\{ \bar{C}_{N,M} (\sin m\lambda_E - \sin m\lambda_W) - \right.$$

$$\left. \left. \bar{S}_{N,M} (\cos m\lambda_E - \cos m\lambda_W) \right\} \cdot \int_{\varphi_S'}^{\varphi_N'} \bar{P}_{N,M} (\sin\varphi') \cos\varphi' \, d\varphi \right],$$

where $\Delta\lambda = \lambda_E - \lambda_W$; and r is the geocentric radius to the center of anomaly block. $\bar{C}_{N,M}$ and $\bar{S}_{N,M}$ are the fully normalized potential coefficients of degree n and order m, the $\bar{C}^*_{N,0}$ being reduced by $\bar{C}_{2,0}$ and $\bar{C}_{4,0}$; and $\bar{P}_{N,M}(\sin\varphi')$ are the fully normalized associated Legendre functions of degree n and order m.

The residual mean gravity anomaly $\Delta g'$ of a block referred to the low degree field was computed as:

$$\Delta g' = \Delta g(30, 28) - \Delta g(12, 12) \tag{4.9}$$

These gave the expected values of the residual mean gravity anomalies, against which the predicted values may be compared. 10° equal area and 5° equal area residual mean anomalies were considered according to the subdivision scheme for equal area blocks described in (Hajela, 1974 a, page 28). These will be referred to as simply 10° and 5° anomalies, and it will be understood that we are discussing the residual anomalies referred to the (12, 12) P.C. field.

Figures 4.1 and 4.2 show the anomaly blocks which will be considered in this paper. The anomaly blocks have been numbered for easy reference, separately for 10° and 5° blocks. The particulars of these anomalies are given in Tables 4.1 and 4.2.

Table 4.1
10° Equal Area Mean Residual Anomalies

No.	φ_N°	φ_S°	λ_W°	λ_E°	$\Delta g(30,28)$ mgals	$\Delta g(12,12)$ mgals	$\Delta g'$ mgals
1	50	40	263	277	- 6.82	- 2.89	-3.93
2	40	30	252	264	3.24	5.33	-2.09
3	40	30	264	276	- 5.39	0.04	-5.42
4	40	30	276	288	- 7.24	-14.60	7.36
5	30	20	251	262	6.93	2.13	4.80
6	30	20	262	273	- 2.09	5.44	-7.53
7	30	20	273	284	- 2.67	- 8.83	6.15
8	20	10	257	267	14.22	11.01	3.20
9	20	10	267	278	18.64	15.92	2.72

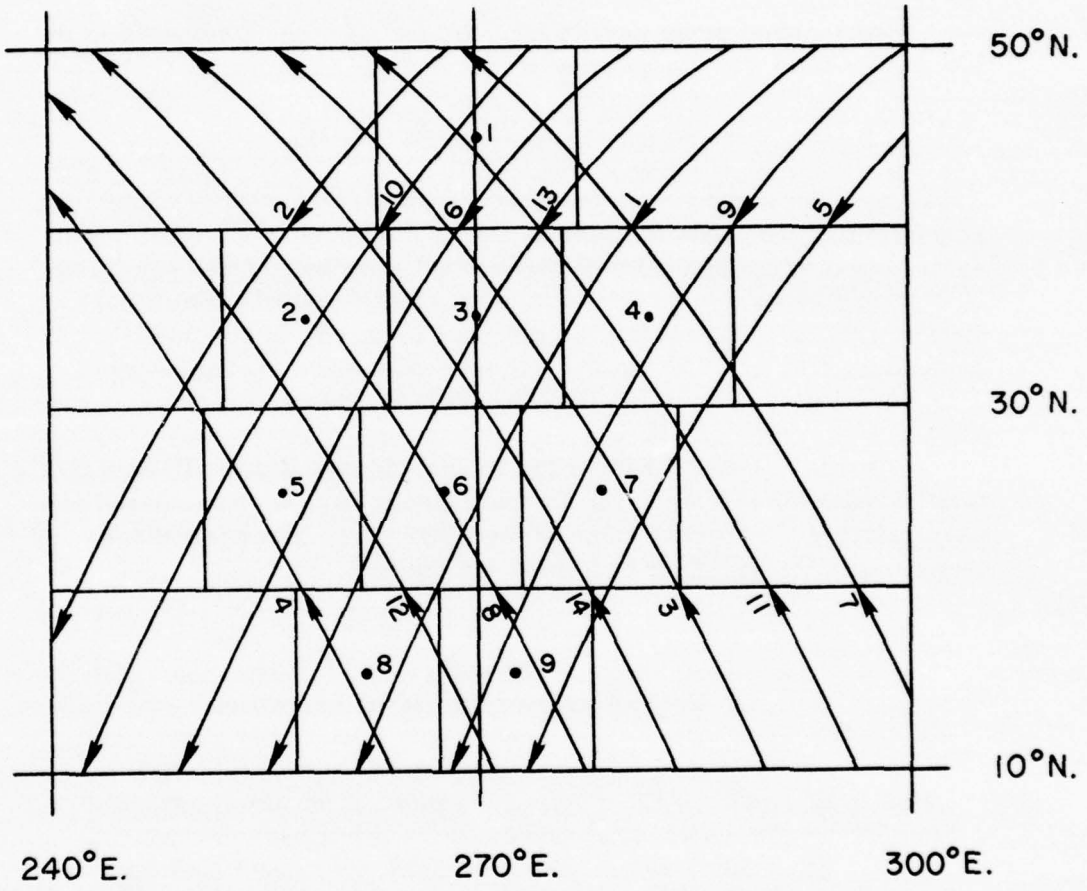

Figure 4.1: Satellite arcs for prediction of
10° residual anomalies no. 1 to 9

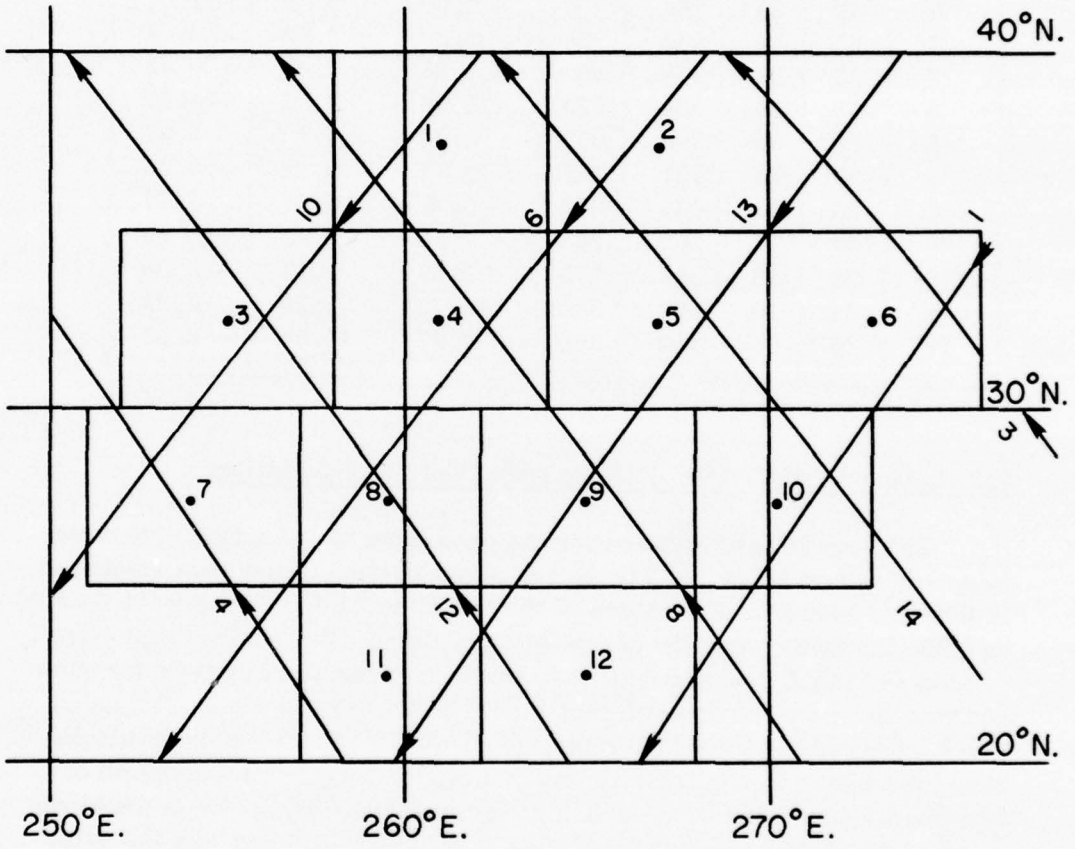

Figure 4.2: Satellite arcs for prediction of
5° residual anomalies no. 1 to 12

Table 4.2
5° Equal Area Mean Residual Anomalies

No.	φ_N°	φ_S°	λ_W°	λ_E°	$\Delta g(30,28)$ mgals	$\Delta g(12,12)$ mgals	$\Delta g'$ mgals
1	40	35	258	264	- 0.13	7.11	- 7.24
2	40	35	264	270	- 7.03	3.98	-11.01
3	35	30	252	258	5.86	2.82	3.04
4	35	30	258	264	- 1.25	5.47	- 6.72
5	35	30	264	270	-11.25	2.82	-14.07
6	35	30	270	276	1.24	- 4.23	5.47
7	30	25	251	257	3.74	- 0.48	4.22
8	30	25	257	262	5.79	4.07	1.72
9	30	25	262	268	- 7.93	5.19	-13.13
10	30	25	268	273	- 6.24	0.34	- 6.58
11	25	20	257	262	15.79	6.56	9.23
12	25	20	262	268	4.97	11.04	- 6.06

4.2 Residual Range Rate Between Relay and Close Satellites

The area of investigation for the prediction of 10° and 5° anomalies was centered on 30° N and 270° E and was a portion of the area discussed in (Hajela, 1974 a). The choice of the initial epoch for defining the inertial coordinate system, and the computation of the inertial position and velocity vectors for the ATS-6 and GEOS-3 satellites at the starting time for each arc was described in that reference, and is therefore not being repeated. The location of the arcs with reference to the 10° and 5° anomaly blocks have been shown in Figures 4.1 and 4.2 respectively. The direction of movement, ascending or descending, of the subsatellite point of the close satellite has also been indicated. The longitudinal spacing was the same for the ascending arcs and the descending arcs. In each case, it was about 6°, which was roughly one-half of the size of the 10° equal area block.

The particulars of the arcs are given in Table 4.3.

Table 4.3
Satellite Arcs Used For Prediction of 10° & 5° Residual Anomalies

Arc No.	Ascending/ Descending Arc	Starting Time*				Duration of Arc		First & Last Subsatellite Pts. For Close Satellite			
		Day	Hour	Min.	Sec.	Min.	Sec.	φ_c°	λ_c°	φ_c°	λ_c°
1	↙	0	09	04	00	22	20	57	306	- 9	250
2	↙	0	10	44	30	19	20	61	292	7	233
3	↖	0	18	44	30	22	20	- 8	299	59	240
4	↖	0	20	25	00	19	30	-14	277	47	236
5	↙	4	08	44	00	20	10	50	305	-12	261
6	↙	4	10	23	30	21	30	57	293	- 6	239
7	↖	4	18	26	00	18	50	7	304	61	247
8	↖	4	20	03	30	20	30	- 9	287	54	239
9	↙	2	08	53	50	21	20	54	306	-10	256
10	↙	2	10	33	00	19	20	61	299	7	240
11	↖	2	18	34	40	21	20	- 3	303	60	242
12	↖	2	20	14	30	19	40	-11	282	50	238
13	↖	6	10	10	50	23	30	60	306	- 9	244
14	↖	6	19	51	00	22	20	-13	295	56	241

* in elapsed time from the initial epoch defining the inertial coordinate system.

The pattern of arcs shown in Figure 4.1 would be available in a period of 6 days, if 2 ascending and 2 descending arcs are observed each day. The sum range rate ($\dot{R}_s$) observations were simulated for about 20 minutes for each arc till the subsatellite point for the close satellite traversed the area roughly bounded by latitudes 10° S. to 60° N. and longitudes 240° E. to 300° E. The $\dot{R}_s$ observations were simulated on a tape separately in the high degree (30, 28) P.C. field and the low degree (12, 12) P.C. reference field. This was done by using the Geodyn program in the data reduction mode, with input as zero $\dot{R}_s$ observations every 10 seconds in the Geodyn binary format (Martin et al, 1975, page C 26.16), for the duration of arc as shown in Table 4.3. The residuals, with their signs reversed, then simulated $\dot{R}_s$ (30, 28) and $\dot{R}_s$ (12, 12) observations at time interval of 10 seconds, depending upon whether the high degree or low degree field was used in the Geodyn program. The residual range rate $\dot{R}_{rc}$ between the relay and close satellites was obtained as in equation (4.1):

$$\dot{R}_{rc} = \dot{R}_s\,(30, 28) - \dot{R}_s\,(12, 12)$$

and written out on another tape in separate files for each arc.

The geodetic coordinates of the ground tracking station for simulating $\dot{R}_s$ observations for all arcs were assumed as:

(4.10)
$$\varphi = 35^\circ\ 11'\ 56\overset{''}{.}096$$
$$\lambda = 277^\circ\ 07'\ 27\overset{''}{.}899$$
$$h = 840.52 \text{ meters}$$

giving a hypothetical tracking station in the vicinity of Rosman, North Carolina.

4.3 Residual Acceleration Between Relay and Close Satellites

We first determine a natural cubic interpolatory spline fitting a finite number of $\dot{R}_{rc}$ values, and then compute the first derivative of the spline at any of the above points, or at an interpolated point between them. The fitted spline would differ depending on the number of $\dot{R}_{rc}$ point values used, eg. 10, 15, or 20 points, and whether we use these points at every 10, 20, or 30 seconds apart. The value of $\ddot{R}_{rc}$ would then also differ depending on the number of $\dot{R}_{rc}$ values used, and their time interval.

If we consider n values of $\dot{R}_{rc}$:

$$\dot{R}_1, \dot{R}_2, \ldots, \dot{R}_n \text{ at time } t_1, t_2, \ldots, t_n,$$

then we define the spline S(t), continuous along with its first ($S'(t)$) and second ($S''(t)$) derivatives on the closed interval $[\dot{R}_1, \dot{R}_n]$, and fulfilling the conditions:

(4.11)
(a) $S(t_i) = \dot{R}_i$; $i = 1, 2, \ldots, n$
(b) $S''(t_1) = S''(t_n) = 0$
(c) S(t) is a cubic polynomial on each interval $[t_i, t_{i+1}]$; $i = 1, 2, \ldots, n-1$

The equation of the spline under the above conditions is given by: (For further details, see (Shampine and Allen, 1973, page 54) . The algorithm described below is based on that reference.)

(4.12)
$$\dot{R}(t) = S_i(t) = \frac{S_i''}{6\Delta t_i}(t_{i+1} - t)^3 + \frac{S_{i-1}''}{6\Delta t_i}(t - t_i)^3$$
$$+ \left(\frac{\dot{R}_{i+1}}{\Delta t_i} - \frac{S_{i+1}''\,\Delta t_i}{6}\right)(t - t_i)$$
$$+ \left(\frac{\dot{R}_i}{\Delta t_i} - \frac{S_i''\Delta t_i}{6}\right)(t_{i+1} - t);$$
$$i = 1, 2, \ldots, n-1,$$

where:

(4.13) $$t_i \le t \le t_{i+1} \quad \text{and} \quad \Delta t_i = t_{i+1} - t_i$$

We are interested in the first derivative of the spline, which is obtained by differentiating equation (4.12), and is given by:

(4.14) $$\ddot{R}(t) = S_i'(t) = -\frac{S_i''}{2\Delta t_i}(t_{i+1}-t)^2 + \frac{S_{i+1}''}{2\Delta t_i}(t-t_i)^2 + \frac{\dot{R}_{i+1}-\dot{R}_i}{\Delta t_i} - \frac{\Delta t_i}{6}\left(S_{i+1}'' - S_i''\right),$$

$$i = 1, 2, \ldots, n-1$$

The second derivatives (S'') of the spline needed in equation (4.14) are computed by the recursive relation:

(4.15) $$S_{i-1}'' = \rho_i S_i'' + \tau_i \; ; \; i=2, \ldots, n$$

starting from $S_n'' = 0$; after we have computed the coefficients ρ_i and τ_i by the following recursive relations (Shampine and Allen, 1973, page 57); starting with $\rho_2 = \tau_2 = 0$ in view of equations (4.11 b) and (4.15):

(4.16) $$\rho_{i+1} = -1 \Big/ \left(\frac{\Delta t_{i-1}}{\Delta t_i}\rho_i + 2\left(1 + \frac{\Delta t_{i-1}}{\Delta t_i}\right)\right)$$

(4.17) $$\tau_{i+1} = \left(d_i - \frac{\Delta t_{i-1}}{\Delta t_i}\tau_i\right) \Big/ \left(\frac{\Delta t_{i-1}}{\Delta t_i}\rho_i + 2\left(1 + \frac{\Delta t_{i-1}}{\Delta t_i}\right)\right) ;$$

$$i = 2, \ldots, n \text{ ; and where}$$

(4.18) $$d_i = \frac{6}{\Delta t_i}\left(\frac{\dot{R}_{i+1}-\dot{R}_i}{\Delta t_i} - \frac{\dot{R}_i - \dot{R}_{i-1}}{\Delta t_{i-1}}\right)$$

The variation of $\ddot{R}(t)$ in equation (4.14) was tested using $\dot{R}_{rc}$ values in 2 arcs (Arcs 1 and 8 in Figure 4.1), when the spline was determined using 5, 10, 15, 20, 25 $\dot{R}_{rc}$ values, which may be 10, 20, 30, 40, 50, 60 seconds apart. The computation of $\ddot{R}(t)$, i.e. $\ddot{R}_{rc}$, was in each case done

at points 10 seconds apart, and the n points (n=5, 10, ..., 25) were equally distributed on each side of the computation point. The last condition of the distribution of points for the spline was of course limited by the first and last $\dot{R}_{rc}$ value in the arc, when the computation points were in the beginning or end of the arc.

It was found that if the spline was fitted on $\dot{R}_{rc}$ values at 20, 30, 40 or 60 seconds apart instead of $\dot{R}_{rc}$ values at every 10 seconds apart, there was a noticeable change in the computed $\ddot{R}_{rc}$ values. This may be seen in Table 4.4 where the computation points are 51 and 55, i.e. 8 min. 20 sec. and 9 min. respectively from the beginning of the arc; number of points ($\dot{R}_{rc}$) used to define the spline are 20 and 15, and the time interval of these $\dot{R}_{rc}$ points are 10, 20, 30, 40 and 60 seconds.

Table 4.4
Variation Of Residual Acceleration Due To Time Interval Of Points For Fitting The Cubic Spline

# Pts. In Spline	Time Interval (Sec.)	$\ddot{R}_{rc}$ in mgals			
		Compn. Pt. In Arc 1		Compn. Pt. In Arc 8	
		51	55	51	55
20	10	0.54559	0.19493	-0.43189	-1.09578
20	20	0.54624	0.19324	-0.43234	-1.09459
20	30	0.54614	0.19352	-0.43314	-1.09415
20	40	0.54640	0.19355	-0.43229	-1.09507
20	60	0.54311	0.19255	-0.43696	-1.09215
15	10	0.54560	0.19490	-0.43184	-1.09581
15	20	0.54607	0.19449	-0.43214	-1.09544
15	30	0.54601	0.19380	-0.43126	-1.09535
15	40	0.54314	0.19416	-0.43115	-1.09518
15	60	0.53866	0.19988	-0.43733	-1.08928

It is therefore advisable to use the $\dot{R}_{rc}$ values at 10 seconds apart to determine the spline. The change in $\ddot{R}_{rc}$ values with this time interval, but with different values of n=5, 10, 15, 18, 20, 25 is shown in Table 4.5. We note that there is little change in $\ddot{R}_{rc}$ after n exceeds 15.

Table 4.5
Variation of Residual Acceleration Due to No. of Points
Used For Fitting The Cubic Spline

# Pts. In Spline	Time Interval (Sec.)	$\ddot{R}_{rc}$ in mgals			
		Compn. Pt. In Arc 1		Compn. Pt. In Arc 8	
		51	55	51	55
25	10	0.54559	0.19494	-0.43189	-1.09578
20	10	0.54559	0.19493	-0.43189	-1.09578
18	10	0.54559	0.19495	-0.43188	-1.09578
15	10	0.54560	0.19490	-0.43184	-1.09581
10	10	0.54573	0.19721	-0.43100	-1.09324
5	10	0.52741	0.22564	-0.48189	-1.05332

The computation of $\ddot{R}_{rc}$ for all arcs was finally done after fitting the cubic spline to 18 $\dot{R}_{rc}$ values at 10 seconds time interval, i.e. for a total time span of 3 minutes. With this fitted spline, $\ddot{R}_{rc}$ was computed at 10 seconds time interval for 6 points in the central 1 minute. The $\ddot{R}_{rc}$ values were thus computed for one minute time span on each occasion using $\dot{R}_{rc}$ values for 3 minutes, centrally straddling the one minute period over which $\ddot{R}_{rc}$ was being computed. Only in the beginning first minute and the last one minute, or the balance portion of the minute, the 3 minute $\dot{R}_{rc}$ values did not encompass the computation points for $\ddot{R}_{rc}$ centrally. It was however found that due to condition (4.11b), the $\ddot{R}_{rc}$ values in the beginning and the end of the arc are much less sensitive to the number of points used for fitting the spline.

The $\ddot{R}_{rc}$ values were written out on tape, one file for each arc, at 10 seconds time interval throughout the duration of arc as given in Table 4.3.

4.4 Radial Derivative of the Disturbing Potential

The ephemeris for the relay and close satellites were written out on tape in the low degree (12, 12) P.C. field by the Geodyn program as described in the beginning of Section 4. The ephemeris provided the inertial position and velocity vectors, and the geodetic latitude , longitude and height of both satellites at 10 seconds time interval. The information for all arcs being processed in a run was available on the same file on the tape, along with headings and arc summaries suitable for printer output. The ephemeris information was extracted out separately for each arc, and written on separate files on another tape.

With the inertial position coordinates of both relay and close satellites available in each arc at 10 seconds time interval, the cosine of the angle between the radial direction at the close satellite and the direction from the close satellite to the relay satellite could be computed at any time according to equation (4.3). Again, with the $\ddot{R}_{rc}$ values available at the same times, as described in the end of Sec. 4.3, the radial derivative of the disturbing potential $(\partial T/\partial r)_c$ at the close satellite could be computed using equation (4.4).

The ephemeris information for each arc, and the residual acceleration $\ddot{R}_{rc}$ values for each arc, could then be merged together to provide all the data required for predicting the residual anomalies. The pertinent information consists of time; geodetic latitude φ_c, longitude λ_c and height h_c of the close satellite; and $(\partial T/\partial r)_c$ values. This was written out at 10 seconds time interval, one file for each arc for the duration given in Table 4.3, on the final data tape to be used for the prediction of residual anomalies.

The algorithms for the prediction of residual anomalies have been described in Sections 2 and 3. The actual prediction tests using the final data tape will be described in Sections 5 and 6.

5. Prediction of 10° Equal Area Residual Anomalies

We will now examine the prediction of 10° residual anomalies using the $(\partial T/\partial r)_c$ values simulated in the previous section. The expected value of the anomalies, $E(\Delta g')$, has been given in Table 4.1. The estimated value, $\hat{\Delta g}'$, of a particular anomaly is computed from:

$$\hat{\Delta g}' = \underline{C}^{T}_{\Delta g' T_r} \left(\underline{\underline{C}}_{T_r T_r} + \underline{\underline{D}}\right)^{-1} \underline{T}_r \qquad (5.1)$$

where $\underline{T}_r \equiv (\partial T/\partial r)_c$ is a vector of a finite number of $(\partial T/\partial r)_c$ values used for estimating the anomaly, with an assumed noise matrix $\underline{\underline{D}}$ and the covariance matrix $\underline{\underline{C}}_{T_r T_r}$, and $\underline{C}_{\Delta g' T_r}$ represents the transpose of the vector of covariances between the anomaly block being estimated and the $\underline{T}_r$ vector.

The computation of $\underline{C}_{\Delta g' T_r}$ and $\underline{\underline{C}}_{T_r T_r}$ was discussed in Section 2. We now assume a diagonal noise matrix $\underline{\underline{D}}$ with all elements the same, and equal to the square of the assumed standard deviation of data, $\underline{T}_r$. We will later consider the effect on the prediction, of various assumed values of the standard deviation of the data.

The number of data points, $(\partial T/\partial r)_c$ values in the vector $\underline{T}_r$, depends on the spherical distance, ψ, from the center of the anomaly block within which the data is considered. Denoting the geodetic latitude and longitude of the center of anomaly block as φ'_g and λ'_g, and those of a $(\partial T/\partial r)_c$ data point as φ_c, λ_c; the value of ψ is given (Heiskanen and Moritz, equation 2-168):

$$\psi = \cos^{-1}\left[\sin\varphi'_g \sin\varphi_c + \cos\varphi'_g \cos\varphi_c \cos(\lambda_c - \lambda'_g)\right] \tag{5.2}$$

The number of data points will also depend on whether we consider each data point at 10 seconds time interval along the arc, or use some other time interval, say 30 seconds or 1 minute. And, finally, the number of data points will depend on the longitudinal spacing of arcs. It may be recalled from Figure 4.1 that the longitudinal spacing of ascending, as well as descending, arcs was about one-half of the 10° anomaly block.

We will examine the variation of the prediction depending on the noise matrix, or the assumed standard deviation of the data; and the variation due to number of data points depending primarily on the spherical distance ψ, and also on the time interval, and the longitudinal spacing of arcs.

The quality of the collocation will be examined by the standard deviation, $\hat{\sigma}_{\Delta g'}$, of the estimated anomaly; as well as the anomaly discrepancy, $\epsilon_{\Delta g'}$, and for comparison only, the correlation coefficient, ρ, of the predicted and expected values of the anomalies. These statistics may be computed from:

$$\hat{\sigma}^2_{\Delta g'} = C_o - \underline{C}^T_{\Delta g' T_r} (\underline{\underline{C}}_{T_r T_r} + \underline{\underline{D}})^{-1} \underline{C}_{\Delta g' T_r} \tag{5.3}$$

where C_o is the variance of the anomalies of that block size.

$$\epsilon_{\Delta g'} = \hat{\Delta g}' - E(\Delta g') \tag{5.4}$$

$$\rho = \left(\sum_n \hat{\Delta g}' E(\Delta g')/n\right) \Big/ \left(\left(\sum_n \hat{\Delta g}'^2/n\right)^{1/2} \left(\sum_n (E(\Delta g'))^2/n\right)^{1/2}\right) \tag{5.5}$$

where n is the number of anomalies being predicted.

A low root mean square (R.M.S.) value of the anomaly discrepancy as compared to the mean standard deviation of the predicted anomalies, and a high value of correlation coefficient would prove the feasibility of the prediction method.

5.1 Variation Due to Change in Assumed Standard Deviation of Data

During the simulation of data in Section 4, we did not consider any observational errors on the $\dot{R}_s$ observations. Also, no uncertainty was ascribed to the potential coefficients describing the high degree or low degree gravity field, or to the epoch parameters of the arcs. We therefore simulated perfect data of $(\partial T/\partial r)_c$ values at the positions (Φ_c, λ_c, h_c) of the close satellite at various times, except for any inherent model inadequacy and degeneration in the procedures of obtaining $(\partial T/\partial r)_c$ values from simulated $\dot{R}_s$ observations.

We may now consider this by treating the $\underline{T}_r$ data to have an assumed standard deviation. 6 cases were considered with the standard deviation as 0.0, 0.1, 0.5, 1.0, 2.0, and 5.0 mgals. We present in Table 5.1 the predicted anomaly, $\hat{\Delta g}'$, and the standard deviation of the predicted anomaly, $\hat{\sigma}_{\Delta g}'$, for two 10° anomalies numbered 3 and 6 in Figure 4.1. We also introduce different number of data points by letting the spherical distance, ψ, vary as 5°, 7.5°, 10°, 15°. The time interval of data points was kept as 1 minute throughout, except for an additional test with 30 seconds for $\psi = 5°$. All the 14 arcs in Figure 4.1 were considered.

We first note that with assumed standard deviation of data as 0.0 mgals, though $\hat{\sigma}_{\Delta g}'$ is obtained satisfactorily, the predicted anomaly $\hat{\Delta g}'$ is greatly in error. By comparing equations (5.1) and (5.3), we conclude that the simulated data of $(\partial T/\partial r)_c$ values are not usable with standard deviation as 0.0 mgals. The prediction is improved with standard deviation of data as 0.1 mgals, but is still unstable for varying spherical distance ψ. On the other hand, as the standard deviation of the data is increased beyond 1 mgal, the predicted anomaly, $\hat{\Delta g}'$, is damped off; and this is very clearly noticable with the standard deviation of data as 5 mgals.

To examine this further, the predicted anomaly is plotted against the assumed standard deviation of data in Figure 5.1, where we present three cases of $\psi = 5°$, with time interval of data as 30 seconds and 1 minute; and $\psi = 7.5°$ with time interval of data as 1 minute. The results are plotted not only for 10° anomalies numbered 3 and 6 given in Table 5.1 and whose expected values were negative, but also for anomalies 4 and 7, whose expected values were positive. The predicted anomaly for standard deviation of data as 0.0 mgals has been omitted.

We clearly notice in all cases the damping of predicted anomalies as the standard deviation of data is increased beyond 1 mgal. The somewhat erratic behavior of the predicted anomaly with standard deviation of data as 0.1 mgal is also noted in some cases. The optimum standard deviation of the simulated $(\partial T/\partial r)_c$ data appears from Figure 5.1 to be 0.5 mgals. (This will be found still more noticeable in Figure 6.1 for for the case of 5° anomalies.)

Table 5.1
Prediction of 10° Residual Anomalies Showing Variation Due To Assumed Standard Deviation (S.D.) of Data, Spherical Distance (ψ°) From Center of Anomaly Block, And Time Interval of Data Points

Spherical Radius ψ° & Time Interval of Data	Assumed S. D. of Data (mgals)	Anom. # 3 Expected Value = -5.4 mgals			Anom. # 6 Expected Value = -7.5 mgals		
		# Data Pts.	$\hat{\sigma}_{\Delta g'}$ (mgals)	$\hat{\Delta g}'$	# Data Pts.	$\hat{\sigma}_{\Delta g'}$ (mgals)	$\hat{\Delta g}'$
	0.0		3.2	- 74.2		3.2	- 2.6
$\psi = 5^\circ$	0.1		3.6	- 4.7		3.6	- 8.3
	0.5	18	4.3	- 7.4	16	4.2	- 8.3
30 sec.	1.0		4.6	- 7.1		4.6	- 7.6
	2.0		5.4	- 6.0		5.4	- 6.3
	5.0		7.0	- 3.0		7.1	- 2.9
	0.0		3.6	- 38.6		3.5	- 9.6
$\psi = 5^\circ$	0.1		4.1	- 10.0		3.8	- 8.4
	0.5	8	4.4	- 7.5	6	4.4	- 8.1
1 min.	1.0		5.0	- 6.8		5.0	- 7.3
	2.0		6.1	- 5.0		6.2	- 5.1
	5.0		7.6	- 1.7		7.6	- 1.6
	0.0		3.2	- 12.6		3.2	-30.0
$\psi = 7.5^\circ$	0.1		3.4	- 5.9		3.4	-13.2
	0.5	19	4.2	- 6.4	19	4.1	-10.0
1 min.	1.0		4.9	- 6.2		4.9	- 7.3
	2.0		5.9	- 5.1		5.9	- 4.9
	5.0		7.4	- 2.1		7.4	- 1.8
	0.0		3.0	95.9		3.1	-15.7
$\psi = 10^\circ$	0.1		3.3	- 7.6		3.3	-10.6
	0.5	31	3.9	- 7.0	30	3.9	- 9.6
1 min.	1.0		4.6	- 6.5		4.8	- 7.5
	2.0		5.8	- 5.2		5.9	- 5.0
	5.0		7.4	- 2.1		7.4	- 1.8
	0.0		2.9	-134.7		2.9	-70.0
$\psi = 15^\circ$	0.1		3.2	- 6.6		3.3	-12.2
	0.5	60	3.8	- 7.0	75	3.8	- 9.6
1 min.	1.0		4.4	- 7.3		4.5	- 7.5
	2.0		5.4	- 6.4		5.5	- 5.3
	5.0		7.1	- 3.2		7.1	- 2.2

$\hat{\sigma}_{\Delta g'}$ = Standard deviation (mgals) of predicted 10° residual anomaly
$\hat{\Delta g}'$ = Predicted 10° residual anomaly (mgals)

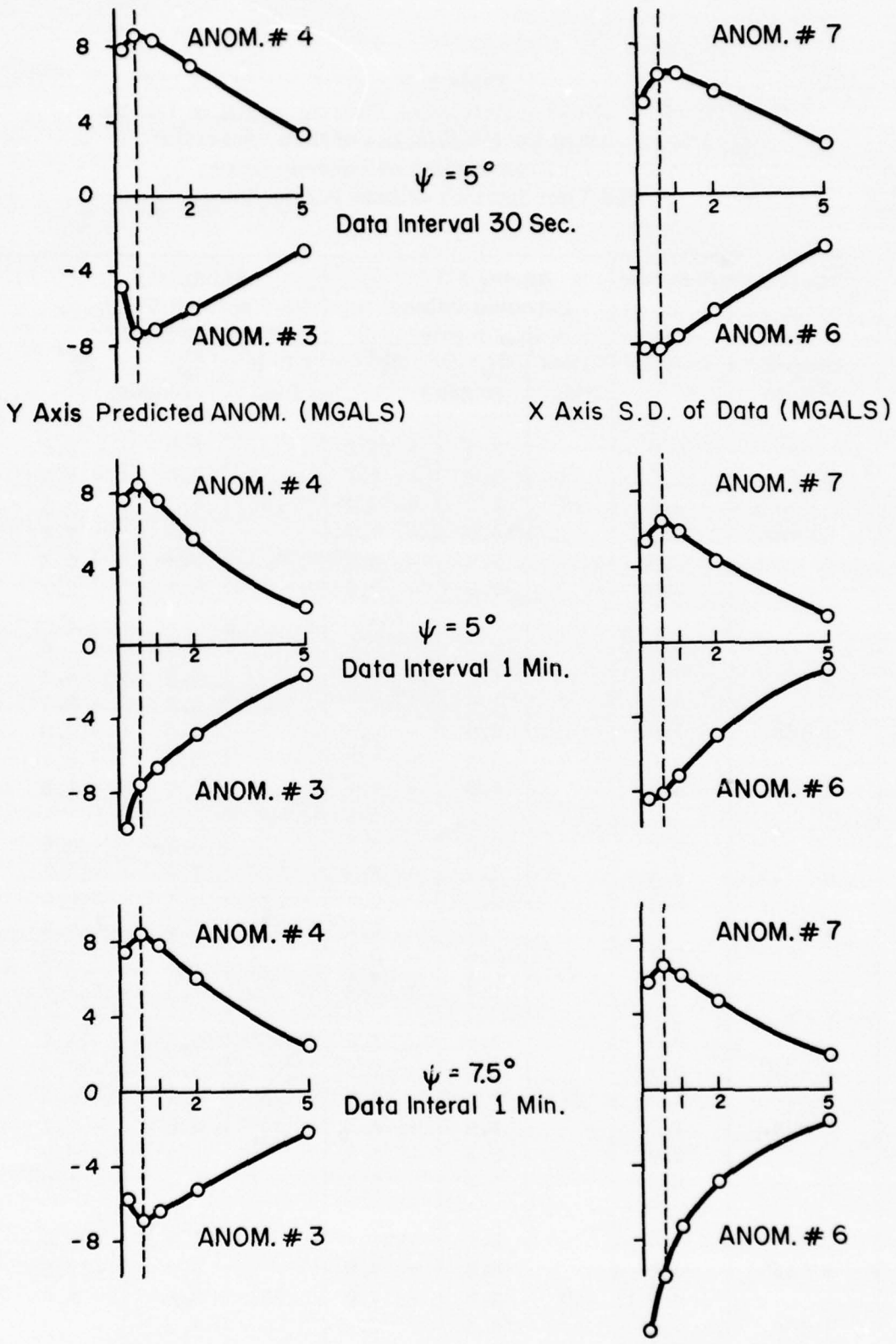

Figure 5.1: Variation of predicted 10° residual anomalies due to change in assumed standard deviation of data

The prediction of other 10° anomalies would thus be examined with standard deviation of data as 0.5 mgals, even though the agreement of predicted anomaly with the expected value may appear to be closer in some cases with standard deviation of data as 1 mgal.

5.2 Variation Due to Change in Spherical Distance From the Center of Anomaly Block

The values for $\hat{\sigma}_{\Delta g'}$ and $\hat{\Delta g}'$ for anomalies 3, 4, 6 and 7 are given in Table 5.2 for the spherical distance $\psi = 5°$, $7.5°$, $10°$ and $15°$. The time interval of data was 1 minute in all cases, and the standard deviation of the data was taken as 0.5 mgals.

Table 5.2
Prediction of 10° Residual Anomalies Showing Variation Due To Spherical Distance ($\psi°$) From Center of Anomaly Block.
Assumed Standard Deviation of Data = 0.5 mgals.
Time Interval of Data = 1 Minute.

ψ	Anom. # 3 $E(\Delta g') = -5.4$ mgals			Anom. # 4 $E(\Delta g') = 7.4$ mgals			Anom. # 6 $E(\Delta g') = -7.5$ mgals			Anom. # 7 $E(\Delta g') = 6.2$ mgals		
	# Pts.	$\hat{\sigma}_{\Delta g'}$	$\hat{\Delta g}'$	# Pts.	$\hat{\sigma}_{\Delta g'}$	$\hat{\Delta g}'$	# Pts.	$\hat{\sigma}_{\Delta g'}$	$\hat{\Delta g}'$	# Pts.	$\hat{\sigma}_{\Delta g'}$	$\hat{\Delta g}'$
5°	7	4.4	-7.5	8	4.4	8.5	6	4.4	- 8.1	7	4.4	6.4
7°.5	19	4.2	-6.4	19	4.2	8.4	19	4.1	-10.0	17	4.2	6.6
10°	38	3.9	-7.0	31	3.9	8.3	30	3.9	- 9.6	30	3.9	6.9
15°	86	3.8	-7.0	60	3.9	8.1	75	3.8	- 9.6	63	3.8	7.1

$\hat{\sigma}_{\Delta g'}$ = Standard deviation (mgals) of predicted 10° residual anomaly

$\hat{\Delta g}'$ = Predicted 10° residual anomaly (mgals)

We note that the improvement in the standard deviation of the predicted anomaly is very slight, from 4.4 mgals to 3.8 mgals, as the number of data points considered (due to increasing ψ) changes from 6 to 8 points at $\psi = 5°$ to 63 to 86 points at $\psi = 15°$.

The estimated anomaly also shows only a slight change due to change in spherical distance ψ. For a standard deviation $\hat{\sigma}_{\Delta g'}$ of about 4 mgals, the range of $\hat{\Delta g'}$ is 1.1, 0.4, 1.9, 0.7 mgals for the 4 anomalies as ψ changes from 5° to 15°. The small range in the predicted values is also shown in Figure 5.2, where the predicted anomaly $\hat{\Delta g'}$ is plotted against spherical distance ψ.

It therefore appears that the prediction of the anomaly block is mainly dependent on the data points which are close to the center of the block, i. e. within $\psi = 5°$ for the 10° blocks. Additional data points beyond $\psi = 5°$ do not contribute any significant information to the predicted anomaly, or significantly lower the standard deviation of the predicted anomaly.

The location of data points with reference to the anomaly block may be seen in Figures 5.3 (a) and (b). These show the data points considered at time interval of 1 minute for the prediction of 10° anomaly number 6, when ψ is taken as 5° and 7.5°. The number of data points increase from 6 to 19, but the additional 13 points lie on the periphery or in the corners of the block and do not contribute any significant information as seen from Table 5.2.

Further tests for the prediction of 10° residual anomalies need then be done only with data points within a spherical distance of 5° from the center of the block.

5.3 Variation Due to Change in Time Interval of Data Points

Figures 5.3 (c) and (d) show the location of data points for the prediction of 10° anomaly number 6, each for $\psi = 5°$, but with time interval of data points as 1 minute and 30 seconds respectively. The number of data points increases from 6 to 16. We present in Table 5.3 the standard deviation $\hat{\sigma}_{\Delta g'}$ of the predicted anomaly and the predicted anomaly $\hat{\Delta g'}$ due to change in time interval of data points for 1 minute to 30 seconds. The information pertains to 10° anomalies numbered 3, 4, 6 and 7.

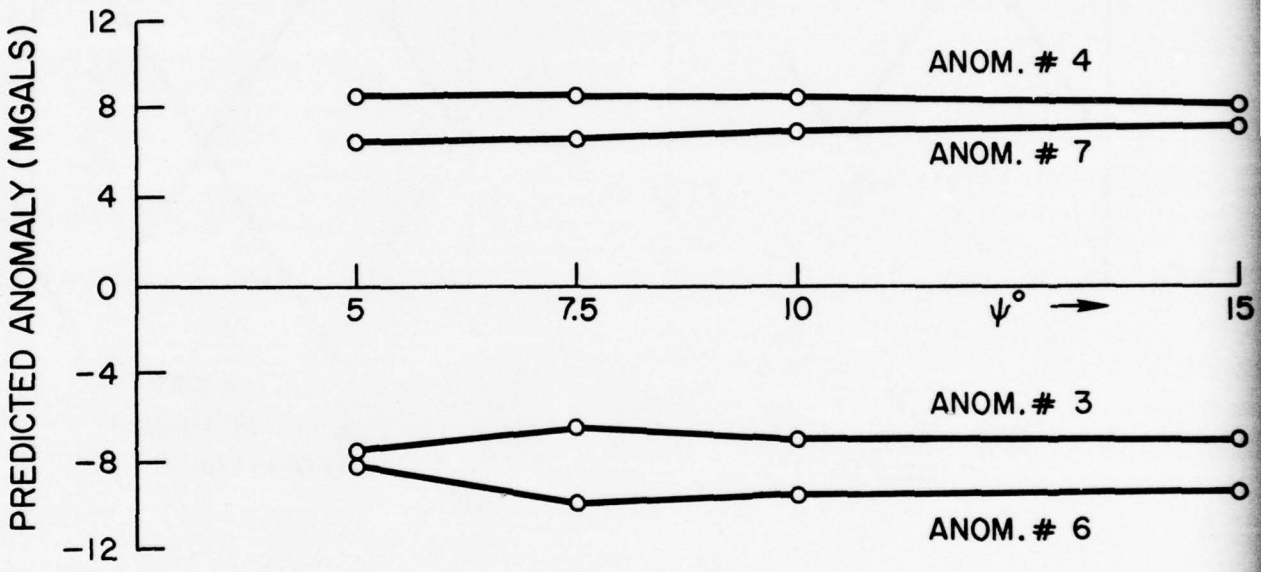

Figure 5.2: Variation of predicted 10° residual anomalies due to change in spherical distance (ψ°) from center of anomaly block up to which data was considered. Data interval was 1 minute. Standard deviation of data was assumed as 0.5 mgals.

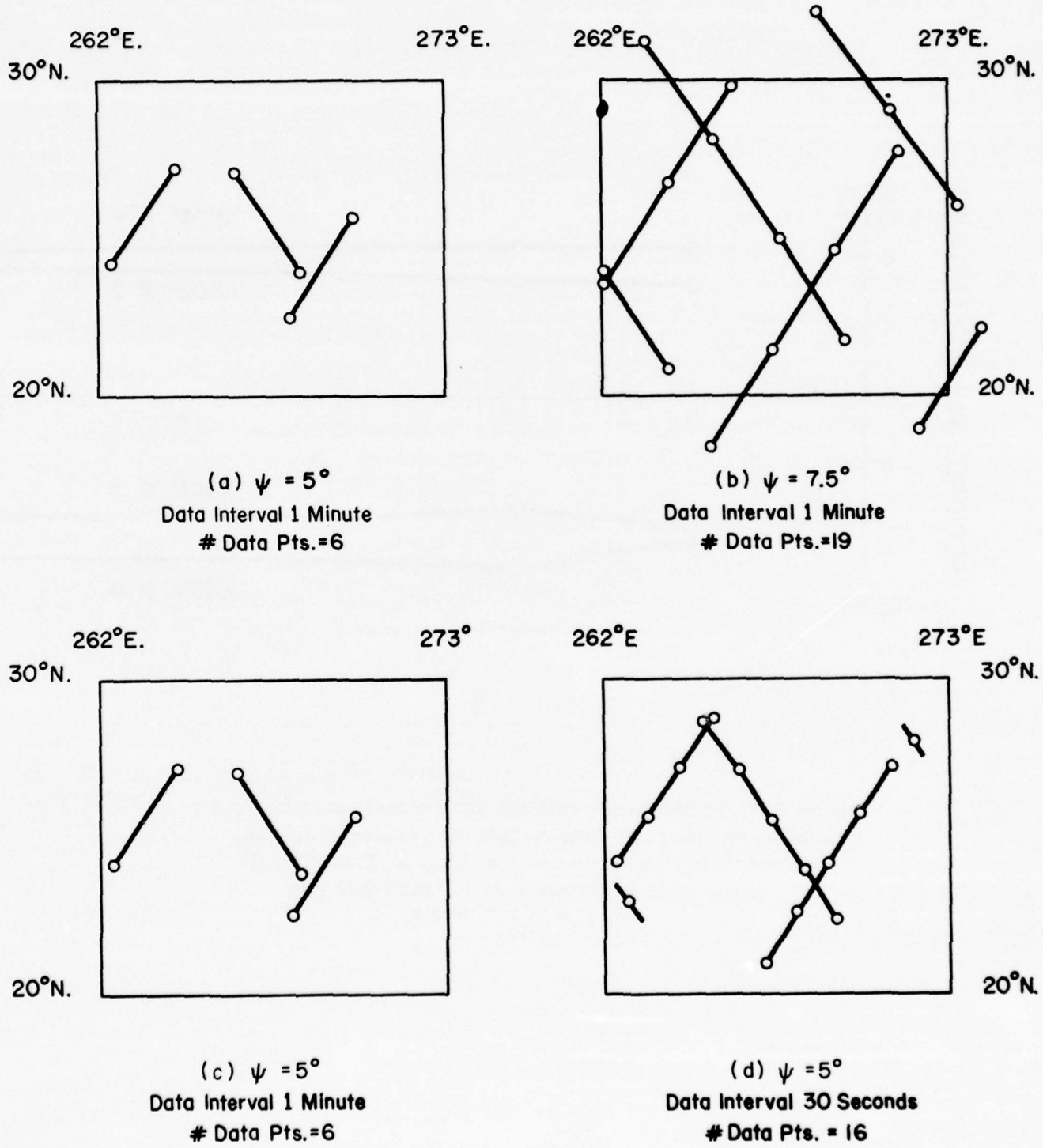

Figure 5.3: Location of data points for prediction of 10° residual anomaly no. 6

Table 5.3
Prediction of 10° Residual Anomalies Showing Variation Due To Time Interval of Data Points. Spherical Distance From Center of Anomaly Block = 5°. Assumed Standard Deviation of Data = 0.5 mgals.

Time Interval of Data Pts. (sec.)	Anom. # 3 $E(\Delta g') = -5.4$ mgals			Anom. # 4 $E(\Delta g') = 7.4$ mgals			Anom. # 6 $E(\Delta g') = -7.5$ mgals			Anom. # 7 $E(\Delta g') = 6.2$ mgals		
	# Pts.	$\hat{\sigma}_{\Delta g'}$	$\Delta\hat{g}'$	# Pts.	$\hat{\sigma}_{\Delta g'}$	$\Delta\hat{g}'$	# Pts.	$\hat{\sigma}_{\Delta g'}$	$\Delta g'$	# Pts.	$\hat{\sigma}_{\Delta g'}$	$\Delta\hat{g}'$
60	7	4.4	-7.5	8	4.4	8.5	6	4.4	-8.1	7	4.4	6.4
30	19	4.3	-7.4	18	4.2	8.6	16	4.2	-8.3	17	4.3	6.3

$\hat{\sigma}_{\Delta g'}$ = Standard deviation (mgals) of predicted 10° residual anomaly
$\Delta\hat{g}'$ = Predicted 10° residual anomaly (mgals)

It is obvious that the time interval of 1 minute for the data points is adequate for the prediction of 10° residual anomalies.

5.4 Summary of Results

We now present in Table 5.4 the predicted values, $\Delta\hat{g}'$, of 9 10° residual anomalies, and the standard deviation, $\hat{\sigma}_{\Delta g'}$, of the predicted anomalies. The anomaly discrepancy, $\epsilon_{\Delta g'}$, i. e. the discrepancy between the predicted and the expected value according to equation (5.4) is also given in Table 5.4. The expected value of the anomalies was given in Table 4.1, and the location of the anomalies in relation to the satellite arcs was shown in Figure 4.1. We recall that the longitudinal spacing of ascending, and descending arcs, was roughly one-half of the 10° equal area blocks, and that the time interval of $(\partial T/\partial r)_c$ data points was 1 minute. We consider data points within a spherical distance of 5° from the center of anomaly block, and we assume the standard deviation of data as 0.5 mgals.

Table 5.4
Prediction of 10° Residual Anomalies.
Spherical Distance of Data Points From Center of Anomaly Block = 5°
Time Interval of Data Points = 1 Minute. Assumed Standard Deviation of Data = 0.5 mgals.

Anom. No.	φ_N°	φ_S°	λ_W°	λ_E°	$E(\Delta g')$ (mgals)	# Data Pts.	$\hat{\sigma}_{\Delta g'}$ (mgals)	$\hat{\Delta g}'$ (mgals)	$\epsilon_{\Delta g'}$ (mgals)
1	50	40	263	277	-3.93	11	4.32	-0.78	3.15
2	40	30	252	264	-2.09	8	4.38	-0.22	1.87
3	40	30	264	276	-5.42	7	4.41	-7.48	-2.06
4	40	30	276	288	7.36	8	4.38	8.46	1.10
5	30	20	251	262	4.80	6	4.34	0.23	-4.57
6	30	20	262	273	-7.53	6	4.37	-8.10	-0.57
7	30	20	273	284	6.15	7	4.43	6.44	0.29
8	20	10	257	267	3.20	6	4.42	3.41	0.21
9	20	10	267	278	2.72	7	4.26	4.64	1.92

Limits of Anomaly Block φ_N°, φ_S° North & South Latitude in Degrees
λ_W°, λ_E° West & East Longitude in Degrees
$E(\Delta g')$ Expected Value of 10° Residual Anomaly
$\hat{\sigma}_{\Delta g'}$ Standard Deviation of Predicted 10° Residual Anomaly
$\hat{\Delta g}'$ Predicted 10° Residual Anomaly
$\epsilon_{\Delta g'}$ Anomaly Discrepancy = Predicted $\hat{\Delta g}'$ - Expected $E(\Delta g')$

The mean standard deviation of the predicted anomalies was 4.37 mgals, while the root mean square (R. M. S.) value of anomaly discrepancy was 2.21 mgals. Further, as the R. M. S. value of the expected anomalies was 5.15 mgals, the R. M. S. value of anomaly discrepancy is acceptable. The correlation coefficient, ρ, between the predicted and expected values of the 9 anomalies considered, as computed from equation (5.5), was 0.915. We may therefore conclude that the procedures developed for the prediction of 10° residual anomalies are workable.

6. Prediction of 5° Equal Area Residual Anomalies

We first test out the conclusions arrived at in Sections 5.1 to 5.3 for 10° residual anomalies, regarding their applicability in the case of 5° residual anomalies. We then use the considerations, so developed, regarding the standard deviation of the $(\partial T/\partial r)_c$ data and the number of

data points to be used, in predicting 12 5° residual anomalies shown in Figure 4.2. A comparison of the predicted anomalies against the expected values given in Table 4.2 would enable us to examine the anomaly discrepancies according to equation (5.4), and the correlation coefficient, ρ, between the predicted and expected values according to equation (5.5). A low root mean square (R. M. S.) value of anomaly discrepancy in comparison to mean standard deviation of the predicted anomalies, and a high value of the correlation coefficient, ρ, would reinforce our conclusions of the feasibility of the prediction method developed in this paper.

6.1 Variation Due to Change in Assumed Standard Deviation of Data

We again examine 6 values of the assumed standard deviation of $(\partial T/\partial r)_c$ data. These were 0.0, 0.1, 0.5, 1.0, 2.0 and 5.0 mgals as in Section 5.1. The standard deviation of the predicted anomaly, $\hat{\sigma}_{\Delta g'}$, and the predicted anomaly, $\hat{\Delta g'}$, are given in Table 6.1 for two 5° residual anomalies numbered 5 and 9. Because of the smaller area of anomaly block, we consider the time interval of data points as 30 seconds, instead of 1 minute in the case of 10° anomalies. The spherical distance, ψ, from the center of anomaly block within which time data points were considered, was $\psi = 2.5°, 3.5°, 5°, 7.5°, 10°$.

We first note from Table 6.1 that for standard deviation of data as 0.0 mgals, though $\hat{\sigma}_{\Delta g'}$ is obtained satisfactorily, it is not possible to use the data for prediction of 5° anomalies. The somewhat erratic behavior of the predicted anomaly with standard deviation of 0.1 mgals is also noticeable. This, and the damping of the predicted anomaly for standard deviation of data exceeding 1 mgal, is seen very clearly in Figure 6.1, where the predicted anomaly has been plotted against the assumed standard deviation of the data for the spherical distance $\psi = 2.5°$, 3.5° and 5°.

We therefore conclude, as in Section 5.1, that for the simulated $(\partial T/\partial r)_c$ data in Section 4, it is appropriate to use the standard deviation of 0.5 mgals.

6.2 Variation Due to Change in Spherical Distance From the Center of Anomaly Block

The standard deviation of the predicted anomaly, $\hat{\sigma}_{\Delta g'}$, and the predicted anomaly, $\hat{\Delta g'}$, have been shown in Table 6.2 for 4 5° residual anomalies numbered 2, 5, 9 and 12 for the spherical distance $\psi = 2.5°$, 3.5°, 5°, 7.5°, 10°. The time interval of data was 30 seconds in all cases, and the data was assumed to have a standard deviation of 0.5 mgals.

Table 6.1
Prediction of 5° Residual Anomalies Showing Variation Due To Assumed Standard Deviation (S. D.) of Data, and the Spherical Distance (ψ°) From Center of Anomaly Block.

Spherical Radius ψ Time Interval of Data	Assumed S. D. of Data (mgals)	Anom. # 5 Expected Value = -14.1 mgals			Anom. # 9 Expected Value = -13.1 mgals		
		# Data Pts.	$\hat{\sigma}_{\Delta g'}$ (mgals)	$\Delta\hat{g}'$	# Data Pts.	$\hat{\sigma}_{\Delta g'}$ (mgals)	$\Delta\hat{g}'$
	0.0		8.2	214.0		8.0	77.8
$\psi = 2.5^\circ$	0.1		10.6	- 3.2		10.1	-12.0
	0.5	4	10.9	- 13.3	5	10.6	-18.2
30 Sec.	1.0		11.5	- 11.6		11.1	-16.5
	2.0		12.7	- 7.7		12.3	-11.6
	5.0		14.2	- 2.3		13.9	- 3.7
	0.0		6.9	-242.3		7.7	51.0
$\psi = 3.5^\circ$	0.1		9.8	- 6.0		9.8	-10.4
	0.5	8	10.9	- 13.2	6	10.6	-18.1
30 Sec.	1.0		11.3	- 13.2		11.0	-16.8
	2.0		12.2	- 10.4		12.1	-12.5
	5.0		13.9	- 3.9		13.8	- 4.4
	0.0		6.2	-303.9		6.4	50.7
$\psi = 5^\circ$	0.1		8.3	- 9.9		8.1	-16.0
	0.5	18	10.7	- 13.1	15	10.3	-17.8
30 Sec.	1.0		11.3	- 13.6		11.0	-16.8
	2.0		12.0	- 11.9		11.9	-13.5
	5.0		13.6	- 5.9		13.5	- 5.9
	0.0		6.0	-508.7		6.0	298.0
$\psi = 7.5^\circ$	0.1		8.0	- 15.0		7.7	-28.8
	0.5	40	9.6	- 12.0	40	9.4	-21.6
30 Sec.	1.0		10.8	- 12.5		10.6	-17.8
	2.0		12.0	- 11.8		11.8	-13.5
	5.0		13.5	- 6.4		13.4	- 6.6
	0.0		5.9	119.8		6.0	373.7
$\psi = 10^\circ$	0.1		7.6	- 8.6		7.4	-28.5
	0.5	74	9.5	- 12.1	69	9.3	-21.4
30 Sec.	1.0		10.4	- 12.9		10.3	-18.0
	2.0		11.7	- 11.8		11.6	-13.9
	5.0		13.4	- 6.4		13.3	- 6.8

$\hat{\sigma}_{\Delta g'}$ = Standard Deviation (mgals) of Predicted 5° Residual Anomaly

$\Delta\hat{g}'$ = Predicted 5° Residual Anomaly (mgals)

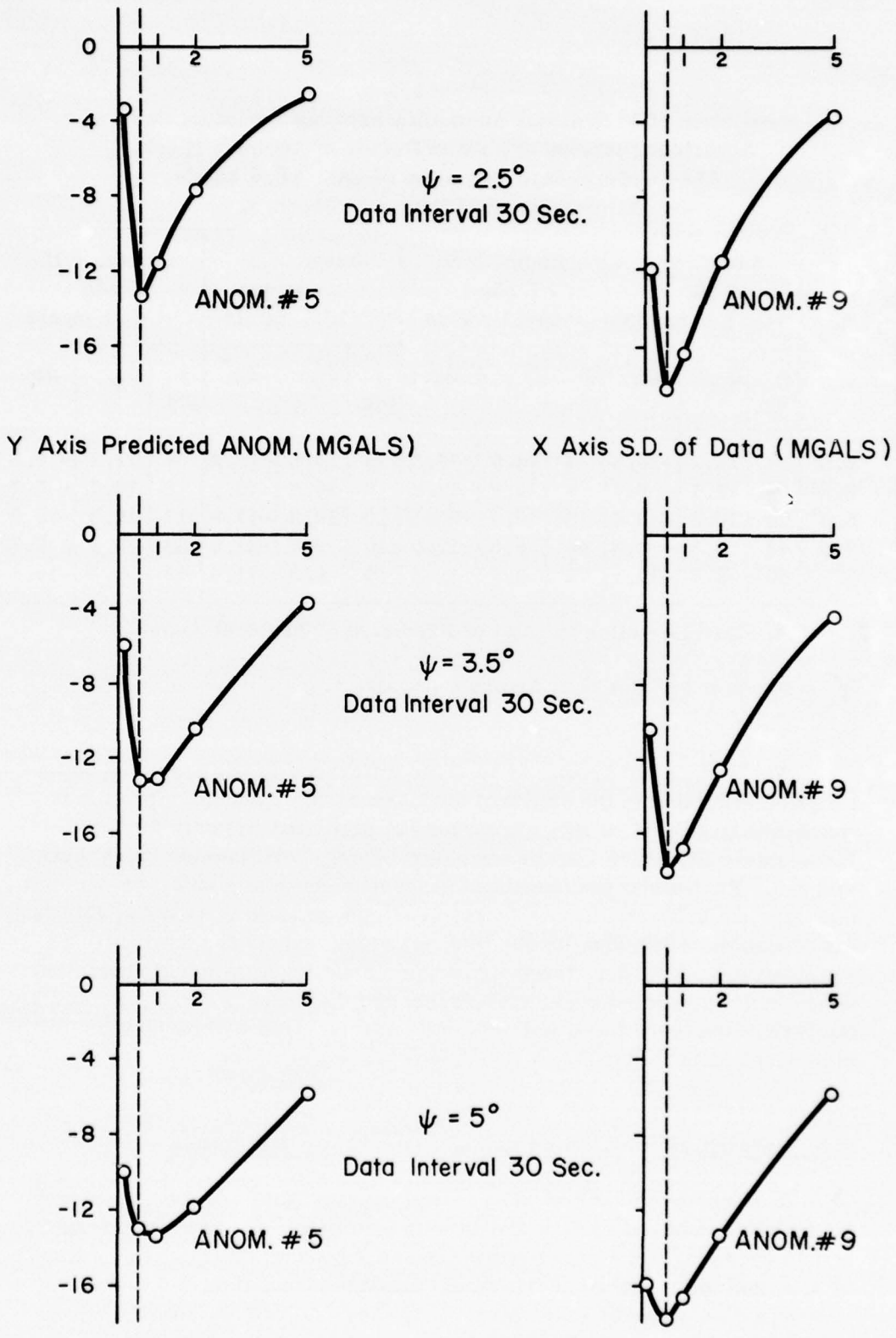

Figure 6.1: Variation of predicted 5° residual anomalies due to change in assumed standard deviation of data

Table 6.2
Prediction of 5° Residual Anomalies Showing Variation Due To
Spherical Distance (ψ°) From Center of Anomaly Block.
Assumed Standard Deviation of Data = 0.5 mgals.
Time Interval of Data = 30 Seconds.

ψ	Anom. # 2 E ($\Delta g'$) = -11.0 mgals			Anom. # 5 E ($\Delta g'$) = -14.1 mgals			Anom. # 9 E ($\Delta g'$) = -13.1 mgals			Anom. # 12 E ($\Delta g'$) = -6.1 mgals		
	# Pts.	$\hat{\sigma}_{\Delta g'}$	$\Delta\hat{g}'$	# Pts.	$\hat{\sigma}_{\Delta g'}$	$\Delta g'$	# Pts.	$\hat{\sigma}_{\Delta g'}$	$\Delta g'$	# Pts.	$\hat{\sigma}_{\Delta g'}$	$\Delta g'$
2.5°	4	11.2	-10.6	4	10.9	-13.3	5	10.6	-18.2	2	11.1	- 3.6
3.5°	9	11.1	- 9.7	8	10.9	-13.2	6	10.6	-18.1	8	10.7	- 5.7
5.0°	20	10.9	- 8.0	18	10.7	-13.1	15	10.3	-17.8	17	10.5	- 5.9
7.5°	44	9.8	- 9.8	40	9.6	-12.0	40	9.4	-21.6	33	9.6	- 7.1
10°	80	9.7	-11.1	74	9.5	-12.1	69	9.3	-21.4	68	9.3	-10.1

$\hat{\sigma}_{\Delta g'}$ = Standard Deviation (mgals) of Predicted 5° Residual Anomaly

$\Delta\hat{g}'$ = Predicted 5° Residual Anomaly (mgals)

There does not appear to be much difference in the predicted anomaly, or much reduction in the standard deviation as the spherical distance is increased from 2.5° to 10°, except for the predicted anomaly for $\psi = 2.5^\circ$ for anomaly 12, which may be explained by only 2 data points being considered. Because of the likelihood of insufficient data points, we may not consider $\psi = 2.5^\circ$, but $\psi = 3.5^\circ$ and 5.0° appear to be equally suitable for predicting the 5° residual anomalies. Further tests will accordingly be reported with $\psi = 3.5^\circ$. However, when all the 12 5° residual anomalies were finally predicted considering spherical distances $\psi = 3.5^\circ$, 5°, 7.5°; the latter sets were found to be slightly better. This will be further elaborated in Section 6.4.

6.3 Variation Due to Change in Time Interval of Data Points

We present the values of $\hat{\sigma}_{\Delta g'}$ and $\Delta g'$ in Table 6.3 for 5° residual anomalies numbered 2, 5, 9 and 12 with time interval of data points as 30 and 10 seconds. Data points were considered within the spherical distance of 3.5° and the standard deviation of data was assumed as 0.5 mgals.

Table 6.3
Prediction of 5° Residual Anomalies Showing Variation Due To Time Interval of Data Points Spherical Distance From Center of Anomaly Block = 3.5°.
Assumed Standard Deviation of Data = 0.5 mgals.

Time Interval of Data Pts. (Sec.)	Anom. # 2 E ($\Delta g'$) = -11.0 mgals			Anom. # 5 E ($\Delta g'$) = -14.1 mgals			Anom. # 9 E ($\Delta g'$) = -13.1 mgals			Anom. # 12 E ($\Delta g'$) = -6.1 mgals		
	# Pts.	$\hat{\sigma}_{\Delta g'}$	$\Delta\hat{g}'$	# Pts.	$\hat{\sigma}_{\Delta g'}$	$\Delta\hat{g}'$	# Pts.	$\hat{\sigma}_{\Delta g'}$	$\Delta\hat{g}'$	# Pts.	$\hat{\sigma}_{\Delta g'}$	$\Delta\hat{g}'$
30	9	11.1	- 9.7	8	10.9	-13.2	6	10.6	-18.1	8	10.7	-5.7
10	29	10.9	-10.3	28	10.5	-11.1	22	10.3	-16.8	28	10.4	-4.7

$\hat{\sigma}_{\Delta g'}$ = Standard Deviation (mgals) of Predicted 5° Residual Anomaly

$\Delta g'$ = Predicted 5° Residual Anomaly (mgals)

It is obvious that the time interval of 30 seconds is adequate for the data points for the prediction of 5° residual anomalies, and no significant advantage is gained by the increase in the number of data points due to the reduction in the time interval of data points from 30 seconds to 10 seconds. The location of data points has been shown in Figures 6.2 (a) and (b) for residual anomaly number 9 with the time interval of data as 30 and 10 seconds respectively.

We recall from Figure 4.2 that the longitudinal spacing of arcs was roughly the same as the 5° anomaly block size, while in the case of prediction of 10° anomalies, the longitudinal spacing of arcs was one-half of the size of 10° block. Additional satellite arcs were then simulated till the longitudinal spacing of ascending, and descending, arcs was one-half of the 5° anomaly block. The location of data points with this increased density of arcs has been shown in Figure 6.2 (c) for anomaly number 9 with $\psi = 3.5°$ and time interval of data points as 30 seconds. In Figure 6.2 (d) we consider the same case but with time interval of data points as 60 seconds.

The values of $\hat{\sigma}_{\Delta g'}$ and $\Delta\hat{g}'$ for anomaly number 9 have been shown in Table 6.4 for the 2 cases in Figures 6.2 (c) and (d), i.e. for longitudinal spacing of arcs one-half of the 5° block size with time interval of data as 30 seconds and 60 seconds. The values for the case in Figure 6.2 (a), i.e. spacing of arcs same as the 5° block size with time interval of data as 30 seconds have also been shown for comparison.

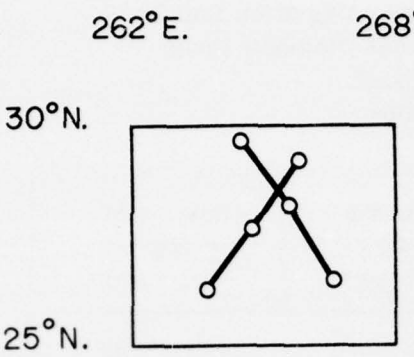

Arc Long. Spacing = Block Size
(a) Data Interval 30 Seconds

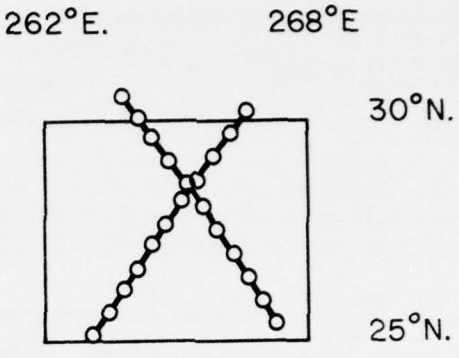

Arc Long. Spacing = Block Size
(b) Data Interval 10 Seconds

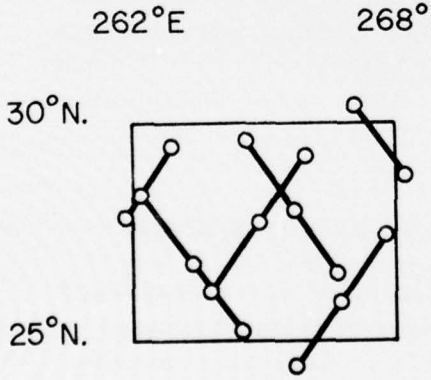

Arc Long Spacing = $\frac{1}{2}$ Block Size
(c) Data Interval 30 Seconds

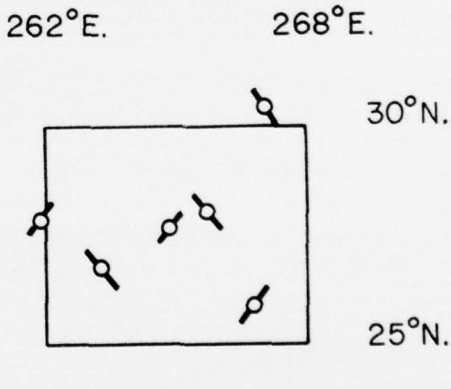

Arc Long Spacing = $\frac{1}{2}$ Block Size
(d) Data Interval 60 Seconds

Figure 6.2: Location of data points for prediction of 5° residual anomaly no. 9. Spherical distance from center of anomaly block = 3°.5

Table 6.4
Prediction of 5° Residual Anomaly No. 9 Showing Variation Due To Change in Number of Data Points With Increased Density of Arcs. Spherical Distance From Center of Anomaly Block = 3.5°. Assumed Standard Deviation of Data = 0.5 mgals

Anom. # 9 $E(\Delta g') = -13.1$ mgals	# Data Pts.	$\hat{\sigma}_{\Delta g'}$ (mgals)	$\Delta g'$ (mgals)
Longitudinal Spacing of Arcs = 1/2 of 5° Block Size			
Time Interval of Data Points = 30 Sec. (Fig. 6.2(c))	16	10.5	-17.1
Time Interval of Data Points = 60 Sec. (Fig. 6.2(d))	6	10.6	-16.8
Longitudinal Spacing of Arcs = Same as 5° Block Size			
Time Interval of Data Points = 30 Sec. (Fig. 6.2(a))	6	10.6	-18.1

From a comparison of Figures 6.2 (a) and (c), it appears that a greater density of observations within the comparatively small size of a 5° anomaly block does not significantly alter the predicted values. Figure 6.2 (d) appears to be basically comparable to Figure 6.2 (a) as though the number of arcs have been increased, the time interval was reduced proportionately.

6.4 Summary of Results

We present in Table 6.5 the standard deviation of the predicted anomaly, $\hat{\sigma}_{\Delta g'}$, the predicted anomaly, $\Delta g'$, and the anomaly discrepancy, $\epsilon_{\Delta g'}$, according to equation (5.4) of all the 12 5° residual anomalies shown in Figure 4.2. The expected value of these anomalies was given in Table 4.2. Data points were used up to a spherical distance of 3.5° with time interval of data points as 30 seconds. The standard deviation of the data was assumed as 0.5 mgals.

Table 6.5
Prediction Of A Local Set Of 5° Residual Anomalies.
Spherical Distance Of Data Points From Center Of Anomaly Block = 3.5°
Time Interval Of Data Points = 30 Sec. Assumed Standard Deviation
Of Data = 0.5 mgals.

Anom. No.	φ_N°	φ_S°	λ_W°	λ_E°	E ($\Delta g'$) (mgals)	# Data Pts.	$\hat{\sigma}_{\Delta g'}$ (mgals)	$\hat{\Delta g}'$ (mgals)	$\epsilon_{\Delta g'}$ (mgals)
1	40	35	258	264	- 7.24	11	11.1	- 1.70	5.54
2	40	35	264	270	-11.01	9	11.1	- 9.69	1.32
3	35	30	252	258	3.04	6	10.8	2.59	-0.45
4	35	30	258	264	- 6.72	6	10.9	-12.55	-5.83
5	35	30	264	270	-14.07	8	10.9	-13.22	0.85
6	35	30	270	276	5.47	8	11.0	1.57	-3.90
7	30	25	251	257	4.22	7	10.6	1.71	-2.51
8	30	25	257	262	1.72	7	11.2	- 6.96	-8.68
9	30	25	262	268	-13.13	6	10.6	-18.08	-4.95
10	30	25	268	273	- 6.58	6	11.4	- 1.15	5.43
11	25	20	257	262	9.23	8	11.4	- 0.28	-9.51
12	25	20	262	268	- 6.06	8	10.7	- 5.66	0.40

Limits of Anomaly Block φ_N°, φ_S° North & South Latitude in Degrees
λ_W°, λ_E° West & East Longitude in Degrees
E ($\Delta g'$) Expected Value of 5° Residual Anomaly
$\hat{\sigma}_{\Delta g'}$ Standard Deviation of Predicted 5° Residual Anomaly
$\hat{\Delta g}'$ Predicted 5° Residual Anomaly
$\epsilon_{\Delta g'}$ Anomaly Discrepancy = Predicted $\Delta g'$ - Expected E($\Delta g'$)

The mean standard deviation of the predicted anomalies was 11.0 mgals, while the root mean square (RMS) anomaly discrepancy was 5.1 mgals. The latter value was therefore acceptable, considering that the R. M. S. value of expected anomalies was 8.2 mgals. The correlation coefficient of the predicted and the expected values of the 12 anomalies, as computed from equation (5.5), was 0.81. The anomaly discrepancy and the correlation coefficient indicate satisfactory prediction of 5° residual anomalies. However, we wish to examine if these could be improved further.

The 12 5° residual anomalies were predicted again using data up to spherical distances $\psi = 5°$ and 7.5°. The time interval of data, and the assumed standard deviation of the data was retained the same as in the case of Table 6.5 with $\psi = 3.5°$. The results of these tests are given in Table 6.6, showing the anomaly discrepancies, $\epsilon_{\Delta g'}$, and the standard deviations, $\sigma_{\Delta g'}$, of the 12 predicted anomalies.

Table 6.6
Prediction of a Local Set of 5° Residual Anomalies Showing Variation of Spherical Distance (ψ) of Data Points From Center of Anomaly Block. Time Interval of Data Points = 30 Sec. Assumed Standard Deviation of Data = 0.5 mgals.

Anom. No.	$\psi = 3.5°$			$\psi = 5°$			$\psi = 7.5°$		
	# Data Pts.	$\hat{\sigma}_{\Delta g'}$ (mgals)	$\epsilon_{\Delta g'}$ (mgals)	# Data Pts.	$\hat{\sigma}_{\Delta g'}$ (mgals)	$\epsilon_{\Delta g'}$ (mgals)	# Data Pts.	$\hat{\sigma}_{\Delta g'}$ (mgals)	$\epsilon_{\Delta g'}$ (mgals)
1	11	11.1	5.5	21	10.8	4.3	46	9.8	1.2
2	9	11.1	1.3	20	10.9	3.0	44	9.8	1.2
3	6	10.8	-0.4	16	10.7	-1.0	42	9.5	-1.0
4	6	10.9	-5.8	16	10.7	-4.6	42	9.6	-5.3
5	8	10.9	0.8	18	10.7	1.0	40	9.6	2.1
6	8	11.0	-3.9	18	10.8	-3.3	40	9.7	-1.5
7	7	10.6	-2.5	17	10.3	-2.0	34	9.5	-0.3
8	7	11.2	-8.7	16	10.8	-5.3	40	10.0	-3.0
9	6	10.6	-5.0	15	10.3	-4.7	40	9.4	-8.4
10	6	11.4	5.4	16	11.2	5.2	38	10.1	5.6
11	8	11.4	-9.5	18	11.2	-8.0	32	10.4	-3.9
12	8	10.7	0.4	17	10.5	0.2	33	9.6	-1.1

$\hat{\sigma}_{\Delta g'}$ = Standard Deviation of Predicted 5° Residual Anomaly

$\epsilon_{\Delta g'}$ = Anomaly Discrepancy = Predicted Anomaly - Expected Value of Anomaly

The improvement in standard deviation with increase in the spherical distance, ψ, is only slight. The anomaly discrepancy even shows worsening in some cases, e.g., anomalies numbered 3, 5, 9, 10, 12; and only a marginal improvement in anomalies numbered 2 and 4. However, there is an improvement when we consider the prediction of the whole set of 12 anomalies, as the spherical distance of data points increases from 3.15° to 7.5°. This is seen more clearly in Table 6.7.

Table 6.7
Prediction of a Local Set of 12 5° Residual Anomalies (Figure 4.2) - Summary of Results. Time Interval of Data Points = 30 Sec. Assumed Standard Deviation of Data = 0.5 mgals.

Spherical Distance $\psi°$	Standard Deviation of Predicted Anomalies in mgals			Predicted - Expected Value of Anomalies in mgals			Correlation Coefficient
	Min.	Max.	Mean	Min.	Max.	R. M. S.	(Eqn. (5.5))
3.5	10.6	11.4	10.98	-9.5	5.5	5.07	0.814
5.0	10.3	11.2	10.75	-8.0	5.2	4.14	0.869
7.5	9.4	10.4	9.75	-8.4	5.6	3.73	0.913

Hence, though the prediction of individual 5° residual anomalies does not show significant improvement in using data points beyond a spherical distance of 3.5° from the center of anomaly block, it would be a better strategy while predicting a local set of 5° residual anomalies to use data points up to a spherical distance of 7.5° from the center of each anomaly block.

7. Effect of Uncertainty in Epoch Parameters on the Prediction of Anomalies

During the simulation of sum range rate observations, $\dot{R}_s$, in Section 4, the inertial position and velocity vectors at the initial epoch of each arc were the same for generating the $\dot{R}_s$ (30, 28) and $\dot{R}_s$ (12, 12) observations. The residual range rate between the relay and close satellites, $\dot{R}_{rc}$, computed in equation (4.1); and subsequently the residual acceleration, $\ddot{R}_{rc}$, and the $(\partial T/\partial r)$ data points used for the prediction of 10° and 5° residual anomalies in Sections 5 and 6, had the implicit assumption that the epoch parameters for the arcs were known without any uncertainty. This allowed the testing of procedures for the prediction of anomalies without any 'aliasing' due to uncertainties in the a-priori determined epoch parameters, i.e. the inertial position and velocity vectors at the initial epoch of each arc. In practice, the epoch parameters are determined from ground tracking, and by first carrying out 'inner iteration' (Martin et al, 1975) for each arc with the available observations. Therefore, the epoch parameters are known only approximately, and we would now examine how this would affect the prediction of anomalies with procedures tested in Sections 5 and 6.

We consider this by using different epoch parameters for generating the $\dot{R}_s$ (12, 12) observations from those used for generating the $\dot{R}_s$ (30, 28) observations. We then obtain $\dot{R}_{rc}$, $\ddot{R}_{rc}$ and $(\partial T/\partial r)_c$ values as outlined in Section 4. If we now use these changed $(\partial T/\partial r)_c$ data points for the prediction of 10° and 5° residual anomalies, we would notice the effect on the prediction of the uncertainties in the epoch parameters by the amount of differences introduced in generating the $\dot{R}_s$ (12, 12) observations. The changes in the epoch parameters were introduced only in one coordinate of the inertial position and velocity vectors for each arc to give one test. Thus there were 6 test cases in which the effect on the prediction was examined for change in one of the X_o, Y_o, Z_o, $\dot{X}_o$, $\dot{Y}_o$, $\dot{Z}_o$ coordinates of the close satellite at the initial epoch for each arc. The epoch parameters of the relay satellite were not changed.

We first present the predicted values of 10° and 5° anomalies with the changed $(\partial T/\partial r)_c$ data, and then examine what interpretation may be given to the predicted values, so obtained.

7.1 Effect on the Prediction of 10° Residual Anomalies

We investigate the effect on the prediction of 10° anomaly number 6. The location of the $(\partial T/\partial r)_c$ data points used in Section 5 for predicting this anomaly was shown in Figures 5.3 (a) and (c) within the spherical distance of 5° from the center of the anomaly block, and with the time interval of data as 1 minute. This gave the number of data points as 6, 2 each for Arcs 1, 8 and 13, as may be seen from Figure 4.1. We now change the position and velocity vector of the close satellite, one coordinate at a time, in generating the $\dot{R}_s$ (12, 12) observations for each of Arcs 1, 8 and 13. After repeating the procedures in Section 4 for these 3 arcs, we will get 6 changed data points but at practically the same locations as in Figures 5.3 (a) and (c), because of only small changes in the epoch parameters, as explained below.

We designate the 6 cases of changed $(\partial T/\partial r)_c$ data by letters A to F. The position coordinates were each reduced by 10 meters in their absolute value in Arcs 1, 8 and 13 giving cases A, B and C. Similarly, the velocity coordinates were each reduced by 1 cm/sec in their absolute value in Arcs 1, 8 and 13 giving cases D, E and F. The change by 10 meters in the position coordinates and by 1 cm/sec in the velocity coordinates was considered to give a realistic representation of the uncertainty in the a-prior knowledge of the epoch parameters. Further, as the absolute values of position and velocity coordinates were reduced but as some of these coordinates were positive and some negative, the final effect was a random increase or decrease of the coordinates in the considered arcs 1, 8 and 13. The increase is indicated by a + sign, and the decrease by a - sign in Table 7.1 for each arc in cases A to F. The $(\partial T/\partial r)_c$ values for the 6 data points in Figures 5.3(a) and (c) are shown in Table 7.2 for cases A to F. The values used in the original case in Section 5, when the epoch parameters for the arcs 1, 8 and 13 were not changed, are also shown in Table 7.2.

Table 7.1
Changes in Epoch Parameters for Arcs 1, 8 & 13.

Case Designation	Close Satellite Coordinate	ARC 1	ARC 8	ARC 13
A	X_o	+ 10 m	+ 10 m	+ 10 m
B	Y_o	- 10 m	+ 10 m	- 10 m
C	Z_o	- 10 m	+ 10 m	- 10 m
D	$\dot{X}_o$	- 1 cm/sec	+ 1 cm/sec	- 1 cm/sec
E	$\dot{Y}_o$	- 1 cm/sec	- 1 cm/sec	- 1 cm/sec
F	$\dot{Z}_o$	+ 1 cm/sec	- 1 cm/sec	+ 1 cm/sec

Table 7.2
Changed Data Points Due to Change in Epoch Parameters of Close Satellite For Prediction of 10° Residual Anomaly No. 6. Spherical Distance of Data Points From Center of Anomaly Block = 5°. Time Interval of Data Points = 1 Minute.

Arc No.	Time in Arc		$(\partial T/\partial r)_c$ in mgals						
	Min.	Sec.	Original Case(Sec 5)	Case A	Case B	Case C	Case D	Case E	Case F
1	11	20	0.63	0.11	3.15	3.10	0.56	2.01	-0.87
1	12	20	0.55	-0.11	3.24	2.94	0.62	2.10	-0.95
8	10	20	1.08	2.22	2.90	-0.50	1.20	0.08	1.57
8	11	20	1.97	3.18	3.68	0.25	2.17	0.97	2.67
13	12	00	2.13	2.47	4.79	5.31	1.69	3.71	0.14
13	13	00	1.10	1.39	3.96	4.23	0.76	2.92	-0.89

The standard deviation of the predicted anomaly, $\hat{\sigma}_{\Delta g'}$, and the predicted value, $\hat{\Delta g'}$, of 10° residual anomaly number 9 are shown in Table 7.3 using the 6 data points in Table 7.3 for each of the 6 cases A to F. The values have been tabulated, assuming that the standard deviation of the data points may be 0.0, 0.1, 0.5, 1.0, 2.0 and 5.0 mgals. The corresponding values for the original case in Section 5, when the epoch parameters were not changed, were given in Table 5.1 for $\psi = 5°$ and time interval of data points as 1 minute.

Table 7.3
Prediction of 10° Residual Anomaly No. 6 Showing Variation Due to Change in Epoch Parameters of Close Satellite. Spherical Distance of Data Points From Center of Anomaly Block = 5°. Time Interval of Data Points = 1 Minute. No. of Data Points = 6.

Assumed S. D. of Data	Case A		Case B		Case C		Case D		Case E		Case F	
	$\hat{\sigma}_{\Delta g'}$	$\Delta\hat{g}'$	$\hat{\sigma}_{\Delta g'}$	$\Delta\hat{g}'$	$\hat{\sigma}_{\Delta g'}$	$\Delta\hat{g}'$	$\hat{\sigma}_{\Delta g'}$	$\Delta\hat{g}'$	$\hat{\sigma}_{\Delta g'}$	$\Delta\hat{g}'$	$\hat{\sigma}_{\Delta g'}$	$\Delta\hat{g}'$
0.0	3.5	-48.9	3.5	11.2	3.5	95.2	3.5	-15.0	3.5	53.2	3.5	-62.8
0.1	3.8	-26.8	3.8	- 7.3	3.8	37.9	3.8	-11.6	3.8	18.9	3.8	-31.2
0.5	4.4	-11.6	4.4	-21.7	4.4	- 8.8	4.4	- 8.4	4.4	-8.3	4.4	- 6.0
1.0	5.0	- 9.7	5.0	-20.4	5.0	-11.0	5.0	- 7.3	5.0	-9.2	5.0	- 3.8
2.0	6.2	- 6.7	6.2	-14.4	6.2	- 8.4	6.2	- 5.0	6.2	-6.9	6.2	- 2.2
5.0	7.6	- 2.1	7.6	- 4.6	7.6	- 2.8	7.6	- 1.6	7.6	-2.2	7.6	- 0.7

All Values Are in Mgals

$\hat{\sigma}_{\Delta g'}$ = Standard Deviation of Predicted 10° Residual Anomaly No. 6

$\Delta g'$ = Predicted 10° Residual Anomaly No. 6. E ($\Delta g'$) =-7.5 Mgals

We notice that the standard deviation of the predicted anomaly is the same for all cases A to F, and the original case in Table 5.1, for any particular assumed standard deviation of the data points. This is so as the location of the data points remains practically the same in all cases because of only small changes in the epoch parameters, and there is thus no particular change in any of the quantities in equation (5.3). We also notice as in Section 5.1 that the value of the predicted anomaly is not usable for standard deviation of data as 0.0 mgals. We have to now interpret what standard deviation may be assumed for the data to predict the 10° residual anomaly. This will be done in Section 7.3. We may, however, note that the standard deviation of 2 mgals for the data gives, in general, a close agreement of the predicted value in cases A to F with the expected value of -7.5 mgals.

7.2 Effect on the Prediction of 5° Residual Anomalies

We investigate the effect of uncertainty in epoch parameters of the arcs in the prediction of 5° residual anomaly number 9. Figure 6.2 (a) shows the location of 6 $(\partial T/\partial r)_c$ data points used for predicting this anomaly in Section 6. There were 3 data points each from arcs 8 and 13, as may be seen from Figure 4.2, and these were at time interval of 30 seconds, and within a spherical distance of 3.5° from the center of anomaly block.

We use the same configuration of data points but with the epoch parameters of the close satellite changed during generation of $\dot{R}_s(12, 12)$ observations, as shown in Table 7.1 for arcs 8 and 13 under cases A to F. The changed value of the $(\partial T/\partial r)_c$ data points is shown in Table 7.4 for cases A to F along with the original case in Section 6, when the epoch parameters of arcs 8 and 13 were not changed.

Table 7.4
Changed Data Points Due to Change in Epoch Parameters of Close Satellite For Prediction of 5° Residual Anomaly No. 9. Spherical Distance of Data Points From Center of Anomaly Block = 3.5°. Time Interval of Data Points = 30 Seconds.

Arc No.	Time in Arc		$(\partial T/\partial r)_c$ in mgals						
	Min.	Sec.	Original Case (Sec. 6)	Case A	Case B	Case C	Case D	Case E	Case F
8	11	10	1.87	3.06	3.59	0.17	2.05	0.86	2.53
8	11	40	2.12	3.35	3.78	0.36	2.34	1.12	2.89
8	12	10	2.16	3.42	3.76	0.34	2.41	1.18	3.04
13	11	20	2.37	2.75	4.90	5.58	1.87	3.80	0.40
13	11	50	2.23	2.58	4.86	5.41	1.77	3.77	0.24
13	12	20	1.85	2.17	4.58	5.01	1.44	3.51	-0.13

The 5° residual anomaly number 9 was predicted using the changed data points shown in Table 7.4 under cases A to F, and the values of $\hat{\sigma}_{\Delta g'}$ and $\Delta\hat{g}'$ are given in Table 7.5. The standard deviation of data was assumed to be 0.0, 0.1, 0.5, 1.0, 2.0 and 5.0 mgals. The values of $\hat{\sigma}_{\Delta g'}$ and $\Delta\hat{g}'$ for the original case in Section 6, when the epoch parameters of arcs 8 and 13 were not changed, were given in Table 6.1 for $\psi = 3.5°$ and time interval of data points as 30 seconds.

Table 7.5
Prediction of 5° Residual Anomaly No. 9 Showing Variation Due To Change in Epoch Parameters of Close Satellite. Spherical Distance of Data Points From Center of Anomaly Block = 3.5°. Time Interval of Data Points = 30 Sec. No. of Data Points = 6.

Assumed S. D. of Data	Case A		Case B		Case C		Case D		Case E		Case F	
	$\hat{\sigma}_{\Delta g'}$	$\Delta\hat{g}'$	$\hat{\sigma}_{\Delta g'}$	$\Delta\hat{g}'$	$\hat{\sigma}_{\Delta g'}$	$\Delta\hat{g}'$	$\hat{\sigma}_{\Delta g'}$	$\Delta\hat{g}'$	$\hat{\sigma}_{\Delta g'}$	$\Delta\hat{g}'$	$\hat{\sigma}_{\Delta g'}$	$\Delta\hat{g}'$
0.0	7.7	-45.5	7.7	197.3	7.7	677.6	7.7	-38.9	7.7	361.6	7.7	-301.7
0.1	9.8	-26.7	9.8	- 8.6	9.8	55.8	9.8	-19.9	9.8	22.8	9.8	- 46.2
0.5	10.6	-25.7	10.6	-36.3	10.6	-20.0	10.6	-17.7	10.6	-18.4	10.6	- 15.1
1.0	11.0	-23.6	11.0	-33.9	11.0	-20.6	11.0	-16.2	11.0	-18.1	11.0	- 13.0
2.0	12.1	-17.4	12.1	-25.0	12.1	-15.4	12.1	-11.9	12.1	-13.5	12.1	- 9.6
5.0	13.8	- 6.1	13.8	- 8.8	13.8	- 5.4	13.8	- 4.2	13.8	- 4.7	13.8	- 3.4

All Values Are in Mgals

$\hat{\sigma}_{\Delta g'}$ = Standard Deviation of Predicted 5° Residual Anomaly No. 9

$\Delta\hat{g}'$ = Predicted 5° Residual Anomaly No. 9. $E(\Delta g') = -13.1$ Mgals

We notice as in Section 7.1 that the standard deviation of the predicted anomaly is the same in all cases A to F, and the original case in Table 6.1, for a particular assumed standard deviation of the data, as the location of the data points remains practically the same due to only small changes in the epoch parameters of the arcs. Further, the predicted anomalies are not usable for standard deviation of data as 0.0 mgals. We also note, as in Section 7.1, that there is generally a close agreement of the predicted anomaly with the expected value of -13.1 mgals, when the standard deviation of the data is assumed as 2 mgals.

7.3 Interpretation of Results

The predicted values of 10° residual anomaly number 6 and 5° residual anomaly number 9 are shown in Table 7.6, after extracting these values for the standard deviation of data as 2 mgals from Tables 7.3 and 7.5.

Table 7.6
Predicted Residual 10° Anomaly No. 6 & 5° Anomaly No. 9
Showing Variation Due to Change in Epoch Parameters
of Close Satellite. Assumed Standard Deviation
of Data = 2 Mgals. Predicted Anomaly Values
Extracted From Tables 7.2 & 7.5

Residual Anomaly No.	Predicted Anomaly in Mgals						S. D. of Predicted Anom. (Mgals)
	Case A	Case B	Case C	Case D	Case E	Case F	
10° Anom. # 6 E ($\Delta g'$) = -7.5 Mgals	- 6.7	-14.4	- 8.4	- 5.0	- 6.9	-2.2	For Cases A to F 6.2
5° Anom. # 9 E ($\Delta g'$) = -13.1 Mgals	-17.4	-25.0	-15.4	-11.9	-13.5	-9.6	For Cases A to F 12.1

We find from Table 7.6 that both for the 10° anomaly number 6 and the 5° anomaly number 9, the predicted anomalies in cases A to F lie almost within one standard deviation (last column of Table 7.6) of the expected value (first column of Table 7.6). It therefore appears that even when there is uncertainty up to 10 meters and 1 cm/sec. respectively in the inertial position and velocity coordinates at the initial epoch for the arcs, the predicted anomaly would be within one standard deviation of the expected value. The uncertainty in the epoch parameters, i.e. the inertial position and velocity coordinates X_o, Y_o, Z_o, $\dot{X}_o$, $\dot{Y}_o$, $\dot{Z}_o$ at the initial epoch, for the arcs up to 10 meters and 1 cm/sec respectively, shows up as spurious variations in the $(\partial T/\partial r)_c$ data with a standard deviation of about 2 mgals. We recall that in Sections 5.1 and 6.1, we found that the simulated $(\partial T/\partial r)_c$ data appeared to be impressed with a standard deviation of about 0.5 mgals, when the epoch parameters for the arcs were implicitly considered to be known without any uncertainty. Now when the epoch parameters have uncertainties, but are considered to be known perfectly, the uncertainties masquerade as a larger standard deviation of the $(\partial T/\partial r)_c$ data.

This is further borne out by examining the data used by us in Tables 7.2 and 7.4. The variation of the data at each of the 6 data points, due to the uncertainties in the epoch parameters of the arcs 1, 8 and 13, has been extracted from Table 7.2 and shown in Table 7.7. The sample standard deviation of the data at each of the 6 points as computed from the different values in cases A to F has also been shown in Table 7.7.

Table 7.7
Variation in $(\partial T/\partial r)_c$ Data Due to Change in Epoch Parameters.
Values Extracted From Table 7.2

Data Pt. #	$(\partial T/\partial r)_c$ in Mgals in Cases A to F						Sample S.D. of Data
1	0.11,	3.15,	3.10,	0.56,	2.01,	-0.87	1.66
2	-0.11,	3.24,	2.94,	0.62,	2.10,	-0.95	1.71
3	2.22,	2.90,	-0.50,	1.20,	0.08,	1.57	1.28
4	3.18,	3.68,	0.25,	2.17,	0.97,	2.67	1.32
5	2.47,	4.79,	5.31,	1.69,	3.71,	0.14,	1.96
6	1.39,	3.96,	4.23,	0.76,	2.92,	-0.89	1.51
Mean of Sample Standard Deviation of $(\partial T/\partial r)_c$ Data							1.57

The mean of sample standard deviations of data computed from arcs 8 and 13 in Table 7.4 gave a similar value of 1.6. This value was also computed separately for cases A to C, and cases D to F, in Table 7.2 resulting in 1.7 and 1.4. It therefore appears reasonable to assume that the uncertainties of about 10 meters and 1 cm/sec respectively in the inertial position and velocity coordinates of arcs at the initial epoch may be accounted for by assuming the standard deviation of $(\partial T/\partial r)_c$ data as 2 mgals.

8. Conclusions

The estimation of mean gravity anomalies at the surface of the earth from satellite to satellite tracking sum range rate observations is in tendency unstable. It involves (1) a numerical differentiation which yields accelerations from the range rate data and (2) a continuation of the radial derivative, T_r , of the anomalous potential, derived from the accelerations, downward to the surface of the earth. Both procedures tend to amplify errors in the observations and in the model.

We propose a method that consists of a differentiation of an interpolatary cubic spline derived from the range rate data to determine accelerations (alternative methods are also discussed) and the least squares collocation method for the estimation of the mean gravity anomalies at the surface of the earth from the T_r - data. For a theoretical unique solution the gradient, $\nabla \underline{T}_c$, of the anomalous potential would have to be computed from the relative accelerations, $\ddot{R}_{rc}$, between the close and the relay satellite. But the determination of $\nabla \underline{T}_c$ from the $\ddot{R}_{rc}$ - values would make necessary a simultaneous tracking of the close satellite by at least three relay satellites. For the treatment of the actual situation of having only one relay satellite we propose two approximate solutions.

The approximation used in our simulation study assumed $\nabla \underline{T}_c$ of having only the radial component, T_r . The experiment chosen was satellite to satellite tracking between the GEOS-3 satellite ($h \doteq 850$ km) and the ATS-6 ($h \doteq 36000$ km).

The simulation brought the following results:

-- The proposed method (differentiation of a cubic interpolatory spline followed by least squares collocation) is economical and produced meaningful results.

-- A 10° residual anomaly (with respect to a (12, 12) reference field) can be estimated with a standard deviation of about 4.4 mgals. The input residual anomalies could be well reproduced within this standard deviation. A 5° residual anomaly can be estimated with a standard deviation of about 11.0 mgals. Also here the input residual anomalies could be well reproduced within this standard deviation. We are well aware, however, of the fact that the variance analysis and the simulation study may not give conclusive indications for the real data processing.

-- The preliminary least squares collocation variance analysis shows that an essential improvement of the above results can be achieved either by a densification of the data tracks or even more by using a close satellite with lower altitude (eg. $h \doteq 250$ km). A reduction of the random observation noise level does not very much contribute to an improvement of the estimation.

-- A very encouraging fact is that only satellite data in a very limited area are needed (inside a cap with a radius of about 7.5° spherical distance around the center of the estimated anomaly block). This allows a very economical data processing. In addition, in contrast to least squares adjustment, least squares collocation allows the estimation of each mean gravity anomaly block independent from one another, which allows the recovery of gravity anomalies in restricted areas.

-- The model error mainly caused by the mentioned approximation inherent in the method could be reasonably controlled by assigning a standard deviation of ± 0.5 mgal to the noise-free T_r values.

-- Because of their systematic influence orbital errors may cause a severe problem for all satellite to satellite tracking experiments. In our simulation errors of 10 m in the position or 1 cm/sec in the velocity were assigned to the starting elements of the close satellite. These errors might be considered as an upper limit of errors occuring in a real experiment with dense ground tracking coverage. The estimated anomalies were disturbed but their deviation from the input values is most times still inside the already shown standard deviation.

Considering these results, an application of the presented method to real satellite to satellite tracking observations is the next logical step.

References

Desrochers, G. A., A Study of the Aliasing Effect on Gravitational Potential Coefficients as Determined from Gravity Data, Department of Geodetic Science, Report No. 160, The Ohio State University, Columbus, December 1971.

Hajela, D. P., Adjustment of Mean Earth Ellipsoid Parameters, Department of Geodetic Science, Report No. 215, The Ohio State University, Columbus, December, 1974 b.

Hajela, D. P., Direct Recovery of Mean Gravity Anomalies from Satellite to Satellite Tracking, Department of Geodetic Science, Report No. 218, The Ohio State University, Columbus, 1974 a.

Heiskanen, W. and H. Moritz, Physical Geodesy, S. Freeman, San Francisco, 1967.

Jordan, S. K., Self-Consistent Models for the Gravity Anomaly, Vertical Deflection, and Undulation of the Geoid, J. Geophysical Research, 77, 20, 3660-3670, 1972.

Kaula, W. M., Error Analysis of Earth Physics Satellite Systems, NASA Gr. No. NGR 05-007-280, Final Report, Part I, 1972.

Kaula, W. M., M. E. Parmenter, N. Burkhard, and D. D. Jackson; Applications of Inversion Theory to New Satellite Systems for Determination of the Gravity Field, AFCRL-TR-75-0450, Final Report, 1975.

Martin, C. F., Geodyn Modifications for Satellite to Satellite Tracking and Surface Density Layer Estimation, Wolf Research and Development Corporation, Riverdale, Maryland, 1972.

Martin, T. and J. T. Serelis, Geodyn Operations Description, Volume III, Wolf Research and Development Corporation, Riverdale, Maryland, April, 1975.

Muller, P. M. and W. L. Sjogren, Mascons: Lunar Mass Concentrations, Science, 61, 680-684, 1968.

Rummel, R., Downward Continuation of Gravity Information from Satellite to Satellite Tracking or Satellite Gradiometry in Local Areas, Department of Geodetic Science, Report No. 221, The Ohio State University, Columbus, 1975 a.

Rummel, R., Surface Gravity Anomalies from Satellite to Satellite Tracking or Satellite Gradiometry--A Downward Continuation Problem, paper presented at the Spring Annual Meeting, AGU, 1975 b.

Schwarz, C. R., Gravity Field Refinement by Satellite to Satellite Doppler Tracking, Department of Geodetic Science, Report No. 147, The Ohio State University, Columbus, 1970.

Shampine, L. F. and R. C. Allen, Numerical Computing: An Introduction, Saunders Company, Philadelphia, 1973.

Tscherning, C. C., Covariance Expressions for Second and Lower Order Derivatives of the Anomalous Potential, Department of Geodetic Science, Report No. 225, The Ohio State University, Columbus, 1976.

Tscherning, C. C. and R. H. Rapp, Closed Covariance Expressions for Gravity Anomalies, Geoid Undulations, and Deflections of the Vertical, Implied by Anomaly Degree Variance Models, Department of Geodetic Science, Report No. 208, The Ohio State University, Columbus, 1974.

Wagner, C., et al , Improvement in the Geopotential Derived from Satellite and Surface Data (GEM 7 and GEM 8), NASA document, X-921-76-20, Goddard Space Flight Center, Greenbelt, MD.

Whittaker, E. and G. Robinson, The Calculus of Observations, 5th ed., Dover Publications, New York, 1967.